CHALMERS
UNIVERSITY OF TECHNOLOGY

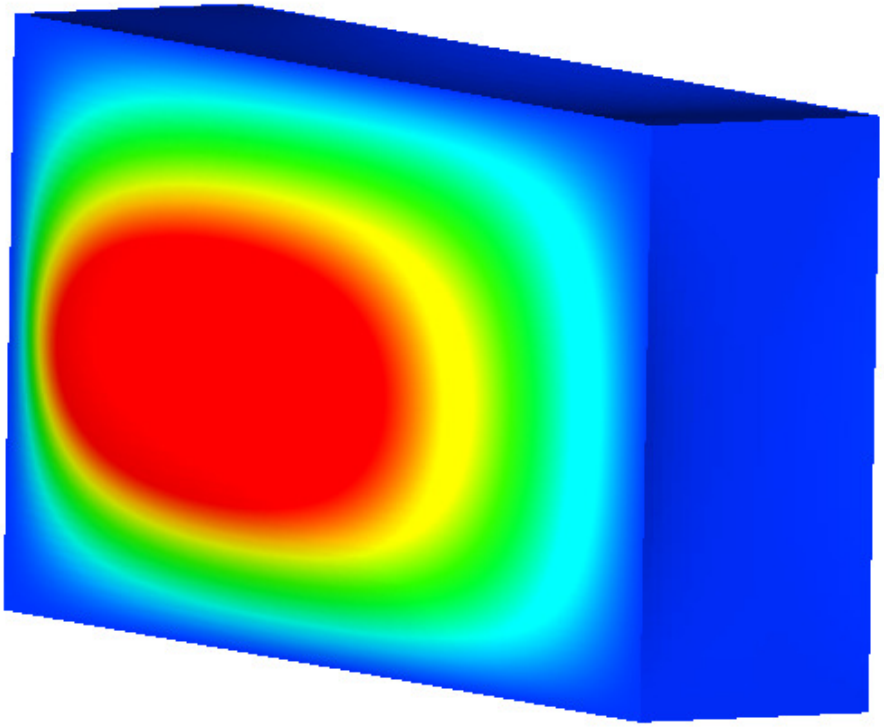

Finite Element Modelling of Cell Swelling for Traction Batteries

Master's thesis in Applied Mechanics

ALBIN KNUTSSON
JONAS TROMBATI

DEPARTMENT OF INDUSTRIAL AND MATERIALS SCIENCE
CHALMERS UNIVERSITY OF TECHNOLOGY
Gothenburg, Sweden 2021
www.chalmers.se

Master's thesis 2021

Finite Element Modelling of Cell Swelling for Traction Batteries

ALBIN KNUTSSON
JONAS TROMBATI

CHALMERS
UNIVERSITY OF TECHNOLOGY

Department of Industrial and Materials Science
Division of Material and Computational Mechanics
Chalmers University of Technology
Gothenburg, Sweden 2021

Finite Element Modelling of Cell Swelling for Traction Batteries
ALBIN KNUTSSON
JONAS TROMBATI

© ALBIN KNUTSSON, 2021.
© JONAS TROMBATI, 2021.

Supervisor: Nandeep Mysore, Volvo Car Corporation
David Carlstedt, Department of Industrial and Materials Science

Examiner: Prof. Leif Asp, Department of Industrial and Materials Science

Master's Thesis 2021
Department of Industrial and Materials Science
Division of Material and Computational Mechanics
Chalmers University of Technology
SE-412 96 Gothenburg
Telephone +46 31 772 1000

Cover: Swelling deformations on a Li-ion battery cell from a Finite Element model.

Printed by Chalmers Reproservice
Gothenburg, Sweden 2021

Finite Element Modelling of Cell Swelling for Traction Batteries
ALBIN KNUTSSON & JONAS TROMBATI
Department of Industrial and Materials Science
Chalmers University of Technology

Abstract

The ongoing electrification of the vehicle fleet creates an increasing demand for high performance traction batteries for electric vehicles. The most common battery type used in electric vehicles today is lithium-ion batteries. During operation the cells in these traction batteries swell. To design a complete battery pack with high volumetric energy efficiency, the cells need to be placed in an optimal manner with minimised margins. In order to achieve this, cell swelling needs to be predicted in the development process.

The main purpose of the project is to study methods on how to empirically model the battery cell swelling behaviour using the Finite Element Method. An established Finite Element model on battery cell swelling open possibilities to evaluate the effects swelling has on complete vehicles, e.g. in crash simulations. Thus, numerical studies were performed with Finite Element models and numerical predictions were compared to provided physical test data (no physical tests were performed in this project).

Different modelling techniques were developed and evaluated. Two types of cell swelling, and a complete module was modelled. Swelling forces on the battery cell were modelled using thermal expansion of the jelly rolls and gas pressure build-up in the cell was modelled using fluid expansion in the cell casing. A complete module model containing multiple cells was developed to evaluate how the swelling affect the module structure. In addition, studies on how the models can be simplified, to reduce complexity and computational demand, were conducted.

The predicted results from the swelling force and gas pressure models coincided well with the physical test data. However, several assumptions were made which need to be validated in future studies. The module model did not coincide well with the available test data. Due to convergence issues some simplifications were made to the model. Thus, further investigation on how to model a complete module is needed. Although some of the models did not yield the desired response, this project is a good foundation for further studies on battery cell swelling models.

Keywords: Finite Element modelling, Battery cell swelling, Lithium-ion battery, Electric vehicles, Battery module, Traction battery

Acknowledgements

This thesis was the final part of the master´s programme Applied Mechanics at Chalmers University of Technology, conducted during the spring semester of 2021. This project was carried out in collaboration with Volvo Cars Corporation (VCC), Gothenburg.

This project was carried out during the odd circumstances of the COVID-19 pandemic. Thanks to our helpful supervisors at Chalmers and VCC it has been possible to finish the project on time. We would like to give an extra thanks to:

David Carlstedt at Chalmers for valuable feedback on the writing process and theoretical parts of the project.

Our examiner Leif Asp for helping out with practicalities at Chalmers and making it possible to finish the thesis on time.

Nandeep Mysore together with the FEM-team at VCC for excellent guidance with Finite Element modelling, debugging and general CAE work.

Marie-Louise Holmer at VCC for giving us the opportunity to carry out our thesis in collaboration with VCC.

Albin Knutsson & Jonas Trombati, Gothenburg, May 2021

Contents

Nomenclature

Abbreviations

EV	Electric vehicle
FE	Finite Element
LFP	Lithium Iron Phosphate
Li-ion	Lithium ion
NMC	Lithium Nickel Manganese Cobalt Oxide
NoTLI	Number of temperature load increments
SEI	Solid Electrolyte Interphase
TLI	Temperature load increments

Symbols

α	Thermal expansion coefficient	[1/°C]
$\hat{E}$	Energy	[J] or [Wh]
μ	Friction coefficient	[-]
ε_T	Thermal strain	[-]
E	Young's modulus	[Pa]
E_{JR}	Young's modulus of jelly rolls	[Pa]
F_{swell}	Swelling force	[N]
h	Thickness	[m]
I	Current	[A]
L	Length	[m]
L_{block}	Block length	[m]
P	Power	[W]
Q	Electric charge	[Ah]
S_f	Scale factor	[-]
T	Temperature	[°C]
t	Time	[s]
T_0	Initial temperature	[°C]
T_{end}	End temperature	[°C]
T_{ref}	Reference temperature	[°C]
T_{start}	Start temperature	[°C]
U	Voltage	[V]
V	Volume	[m^3]
V_0	Initial volume	[m^3]

List of Figures

List of Tables

1
Introduction

1.1 Background

With the ongoing electrification of the vehicle fleet, there is an increasing demand for rechargeable batteries. In 2017, the demand of energy storage in electric vehicles (EVs) accounted for two thirds of the global battery sales [1]. Today, the most common used battery type, in the vehicle industry, is lithium-ion (Li-ion) batteries. Advantages with Li-ion batteries are long cycle life, low self-discharge and high energy density [2]. However, during service the Li-ion cells swell which affects the performance of the batteries and the structures around them.

When assembling a complete battery pack, it is of high importance to foresee this swelling behaviour. Swelling of battery cells results in a pressure on the module walls encasing the cells and affects the space available to allow intrusion in the event of a crash. In addition, it is important to have a high volumetric energy efficiency, i.e. package as many cells as possible in the battery pack. If the swelling behaviour is foreseen, the cells can be placed in an optimal manner with minimised margins.

Li-ion batteries have been commercially available since the early 1990s. In addition to EVs, e.g. smartphones or laptops. Although consumer electronics also requires high performing batteries, the development of EV batteries focus on additional areas. The batteries in EVs are used in more extreme conditions, e.g. larger temperature differences or moist environment. This makes them more prone to swelling compared to consumer electronics. Also, due to the energy requirements of EVs, a large number of cells are needed. Understanding the swelling and the effect it has on the surrounding for this type of application is important, e.g. in the event of a crash a swollen cell is more prone to get punctured.

Efficient modelling strategies for predicting the swelling behaviour of battery cells are lacking. Therefore this thesis investigates how the swelling behaviour of a Li-ion battery cell can be captured in a FE-model. Methods on how experimental data on swelling can be used to capture this behaviour in FE-models are presented. Additionally, suggestions on future work related to modelling of swelling behaviour are discussed.

The Li-ion battery cell that is studied in this project is a member of a complete battery pack. The battery pack contains several modules and each module contains several cells. The cell is a prismatic cell and it consists of two flat jelly rolls which are encased by an aluminium casing. The cell uses a graphite anode, a Lithium Nickel Manganese Cobalt Oxide (NMC) cathode and a liquid electrolyte. The cells are connected in parallel and/or in series depending on what voltage and energy that required for the application.

1.2 Aim and approaches

The aim of this thesis is to establish methods for capturing the swelling behaviour of Li-ion battery cells in a FE-model. These methods describe how one can use physical swelling data to predict the swelling behaviour in a FE-model.

This project was provided with two different types of physical test data for the battery cell: (i) Swelling force on the outside of the battery cell over number of cycles; (ii) Gas pressure inside the battery cell over years. This report presents one method to fit the experimental data on swelling force and one method to fit data for the gas pressure inside the cell. The method for the swelling force will be referred to as M1 in this report and the method for the gas pressure will be referred to as M2. A simplified model of the M1 method was created to reduce the computational resource demand in a full module or battery pack simulation, this concept is referred to as M3.

In addition, studies on a complete module were performed. The project was provided with physical test data for the module in terms of displacements of the end plates. A different swelling force, compared to the one used in M1, was used as input for the cells in the complete module study. The complete module was simplified to only contain one solid block representing all the battery cells. These studies will be referred to as M4 in the report.

1.2.1 M1: Swelling force

The physical test data on the swelling force include all sources contributing to swelling of the cell, e.g. gas build-up and SEI-layer growth. This method uses thermal expansion of the jelly rolls to replicate the swelling of the battery cell. The thermal expansion represents the total swelling, i.e. all the swelling sources included and not only the thermal effects. A reaction force was then obtained in one direction.

1.2.2 M2: Gas pressure

In this method available data on the gas pressure evolution in the battery cell was used. To model this a closed volume containing an incompressible fluid was set up and the gas pressure build-up was simulated with thermal expansion of the fluid.

1.2.3 M3: Simplified geometry

To reduce computational resources needed to solve the swelling force a simplified geometry was created based on the M1 method. The simplification consisted of a solid block, which means that contacts between the jelly rolls and the casing can be neglected.

1.2.4 M4: Battery module

A full detailed module containing multiple battery cells and foam pads was modelled. This model used the M1 method to model the swelling behaviour of the cells. This model was also simplified with the detailed module as a reference. The simplification consisted of replacing the battery cells and foam pads with a solid block using a bulk material representing the battery cells and foam material inside the module, similar to the M3 method.

1.3 Limitations and scope

The limitations and scope of this thesis project are listed below without any specific order.

- Study performed on a single prismatic Li-ion battery cell using two flat jelly rolls and liquid electrolyte.
- Swelling effects modelled on battery cell level, not microscopic level.
- No physical testing performed, only numerical studies are performed.
- Heat transfer and heat generation in the cell are neglected.
- Studied life span of battery cells: $0 - 1500$ cycles. The model is only valid in this range and no comments can be made about the validity of the methods and results outside this range.
- Normalised values, measurements and results, and general schematics of geometries and models used due to confidentiality.
- Developed models are considered empirical since they require test data for each individual type of cell and test condition.
- Three scenarios were investigated: (i) Swelling force; (ii) Gas pressure; (iii) Module deformations.
- The models were developed to be used with commonly available FE-solvers that handles linear thermal expansion and fluid pressure changes.

2
Theory

2.1 Battery

A battery is a device that can store chemical energy. In addition, the chemical energy can be converted to electrical energy. A battery cell can be connected either in serial and/or in parallel to increase the output voltage and/or current. Batteries can either be a single-use battery or a rechargeable battery, which is the one this report will focus on.

2.1.1 Battery cell

A battery cell consists of two electrodes, anode and cathode. These are separated by an electrolyte and a separator. The electrolyte is a solution that allows transportation of ions. It can be a gel, fluid or a solid substance [3]. The separator prevents internal short circuit by separating the two electrodes. In addition, the cell contains current collectors to extract the current and to obtain as efficient transfers of the electrons between the electrodes as possible [4]. Figure 2.1 shows a schematic illustration of a battery cell during charge and discharge.

There are several materials used for the different parts in a Li-ion battery cell. Graphite is a common material for the anode and Lithium Iron Phosphate (LFP) or Lithium Nickel Manganese Cobalt Oxide (NMC), among others, are commonly used for the cathode. Aluminium is often used as the current collector at the cathode and copper at the anode.

A battery cell which is only valid for one discharge is called a primary cell [3]. This type of cells are of galvanic nature which means that the cell can only convert chemical energy to electric energy [4]. Thus, a primary cell is non-rechargeable which make them unusable in EVs. Instead, EVs use cells called secondary cells. This type of cells operates as galvanic cells, just like the primary cells, but in addition to that, the secondary cells can also operate as electrolytic cells [4]. This means that it has the ability to convert chemical energy to electric energy, just like the primary cell, but also vice versa. Thus, the secondary cell is rechargeable and therefore the one used in EVs.

During discharge of a battery, electrons are transported from anode to cathode via the outer circuit, through the external load. To maintain charge balance, ions are transported in the same direction within the electrolyte. Two types of currents are generated due to these flows. One current is generated by the flow of ions and one by the flow of electrons. The current generated by the electrons is the one which powers the external load, e.g. an electric propulsion motor in a car. This process can be seen in Figure 2.1a. Charging is a similar but reversed event where electrons and ions are transported from cathode to anode, which can be seen in Figure 2.1b. To charge the battery cell an external current is applied via the outer circuit e.g. by using a battery charger.

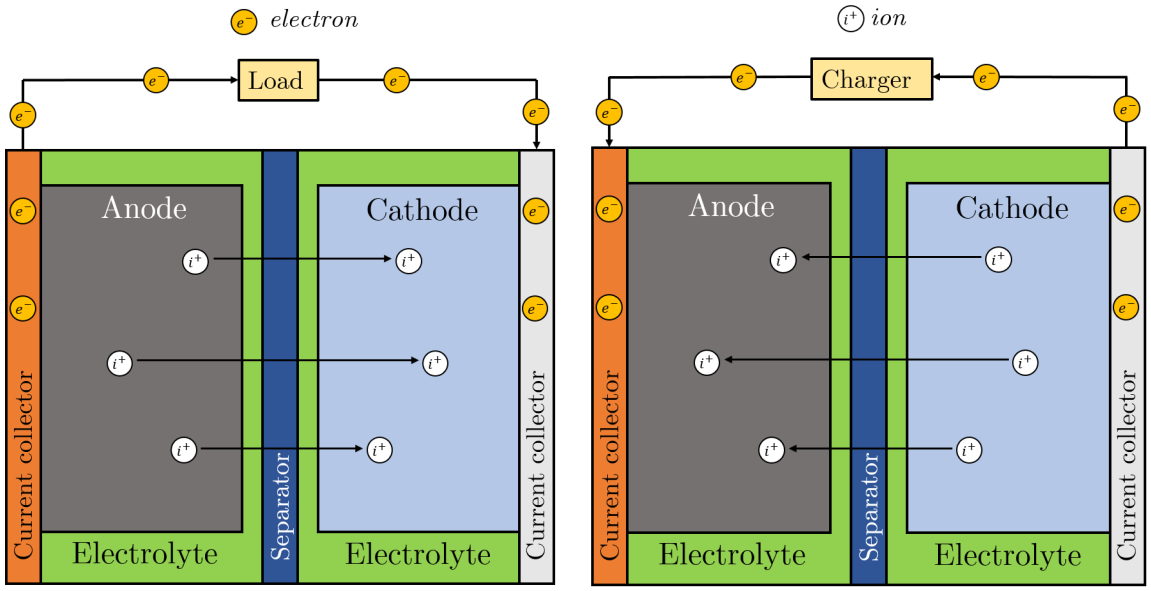

(a) Li-ion battery during discharge. **(b)** Li-ion battery during charge.

Figure 2.1: Discharge (2.1a) and charge (2.1b) of a Li-ion battery cell.

2.1.1.1 Battery cell characteristics

A battery cell have several useful characteristics: voltage U, current I, power P, electric charge Q and energy $\hat{E}$. These characteristics can also be time dependent. Power, electric charge and energy are calculated as

$$P(t) = I(t) \cdot U(t) \tag{2.1}$$

$$Q = \int I(t)\, dt \tag{2.2}$$

$$\hat{E} = \int P(t)\, dt \tag{2.3}$$

where t is the time variable.

2.1.1.2 Battery cell types

A battery cell can be packaged in different ways to suit the application. Figure 2.2 shows three common cell types, prismatic cell, cylindrical cell and pouch cell.

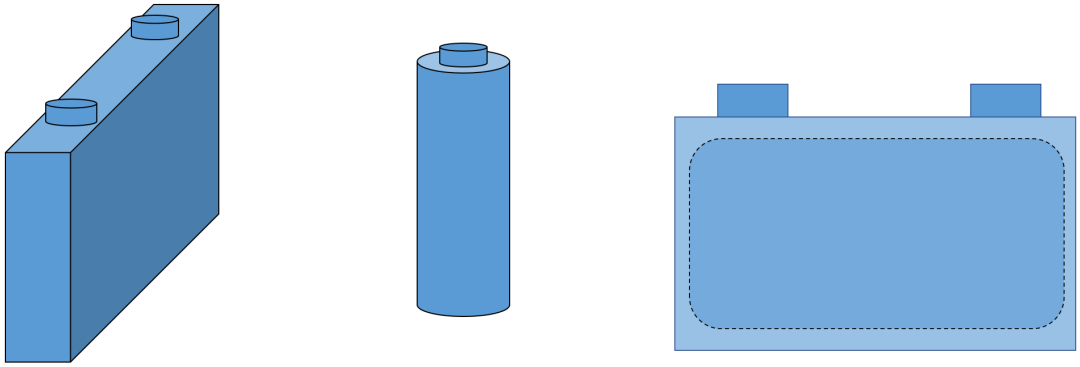

(a) Prismatic cell. **(b)** Cylindrical cell. **(c)** Pouch cell.

Figure 2.2: Different types of cells.

The anode, cathode and separator can be assembled in different ways. These electrode assemblies are commonly called jelly rolls, and typical manufacturing processes are single sheet stacking, Z-stacking, cylindrical winding (cylindrical jelly roll) and prismatic winding (flat jelly roll). The prismatic winding of the electrodes and separator is shown in Figure 2.3. Single sheet stacking, Z-stacking and cylindrical jelly roll are shown in Figure 2.4.

Sheet stacking is when the anodes, cathodes and separators are stacked in an alternating fashion. Z-stacking is similar to single sheet stacking, but the separator is in one continuous piece. Cylindrical and prismatic winding is when the anode, cathode and separator are formed in long sheets, stacked on each other and wound up to either a cylindrical or flat shape. [5]

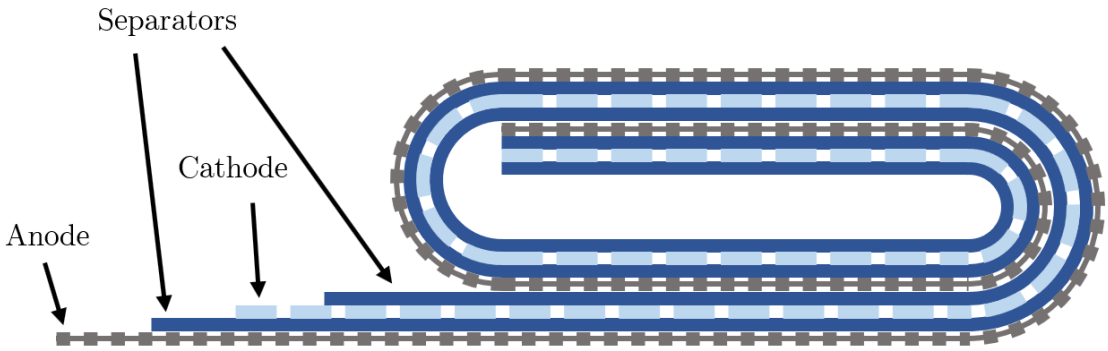

Figure 2.3: Prismatic winding (flat jelly roll) used in prismatic cell.

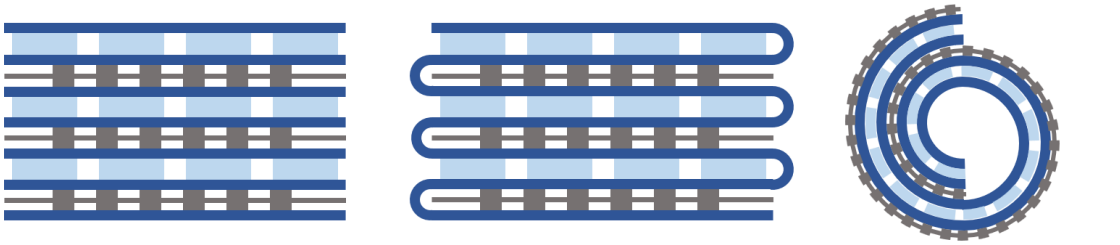

Figure 2.4: Different types of jelly rolls.

The assemblies are inserted into a casing, typically made from stainless steel or aluminium, to protect them from moisture, oxygen and external loads [6]. The prismatic cell has a hard box shaped casing, Figure 2.2a, and the cylindrical cell has a hard casing shaped as a cylinder, Figure 2.2b. Pouch cells uses a different package design, here the anode, cathode and separators are stacked on top of each other and housed in a pouch-bag. The pouch-bag is not a hard case which makes it more flexible and lightweight [7]. Due to the soft housing design, the pouch cells are more prone to swelling which need to be considered when packing the cells in a battery pack.

2.1.2 Battery swelling

Battery swelling is caused by several mechanisms within the battery. There is e.g. swelling due to thermal effects, Solid-Electrolyte Interphase (SEI) layer formation and growth, gassing, plating and intercalation.

2.1.2.1 Thermal swelling

Thermal swelling occurs when the temperature changes e.g. when heat is generated in the battery during charge and discharge. The generated heat originates from chemical reactions and internal resistance in the battery [8]. The demand for shorter charging times requires large currents, which generates more heat in the battery and causes swelling.

2.1.2.2 SEI layer growth

SEI layer is a passivating layer that forms on the electrodes when the electrolyte is reduced through cathodic reactions at the electrode. This layer is necessary since the reaction between electrode and electrolyte is unstable. An initial SEI layer is formed during the first charge/discharge cycle. This layer grows at a slow rate since the initial layer slows down the breakdown of electrolyte. As the SEI layer grows, more cyclable lithium is locked in the layer, which reduces the capacity of the battery. The SEI layer also acts as a resistor with increasing resistance as the layer grows, this resistance causes electrical losses in the form of heat generation [9].

2.1.2.3 Gas generation

In a battery cell, gasses are generated when the electrolyte decomposes [10]. Abusive conditions such as overcharging and overheating increases gas generation in the cell [11]. The gas generation leads to swelling and pressure build-up [12]. It also affects e.g. the cell performance and reduces the cycle lifetime [13].

2.1.2.4 Lithium plating

Metallic lithium formations on the anode surface during charging is called lithium plating. The plating is caused by large currents and low temperature. Large currents cause ions to move quicker than intercalation takes place and low temperatures cause the chemical reactions to slow down [14]. If extensive plating takes place there is a risk of the metallic lithium to form a conductive path through the separator, resulting in an internal short circuit.

2.1.2.5 Intercalation

Intercalation is the process where molecules or ions are inserted in materials with a layered structure. This process happens, e.g. in Li-ion batteries as lithium ions from the cathode are inserted in the graphite anode. Figure 2.5 illustrates this phenomena. When this occurs there is a volume change, i.e. swelling, of the electrode that receives ions [15]. In the ideal case intercalation is fully reversible, but irreversible effects are often observed, mainly due to formation of the SEI layer.[16]

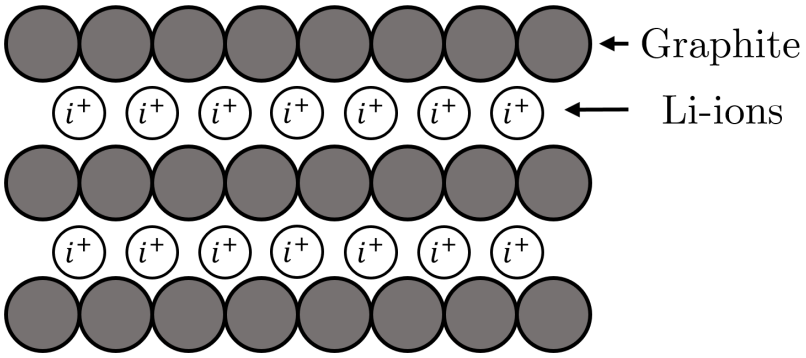

Figure 2.5: Intercalation of Li-ions in the layered structure of a graphite anode.

2.1.3 Battery module

The battery module consists of interconnected battery cells. In order to obtain the required voltage, power, capacity etc., these cells are configured in different ways. For example, cells connected in series increase the voltage and cells connected in parallel increase the capacity. It is also possible to have a combination of cells in series and parallel to obtain a combination of voltage and capacity increase. These combinations use the naming convention (nPmS), where n is the number of cells in parallel and m is the number of cells in series. Examples of the different configurations can be seen in Figure 2.6.

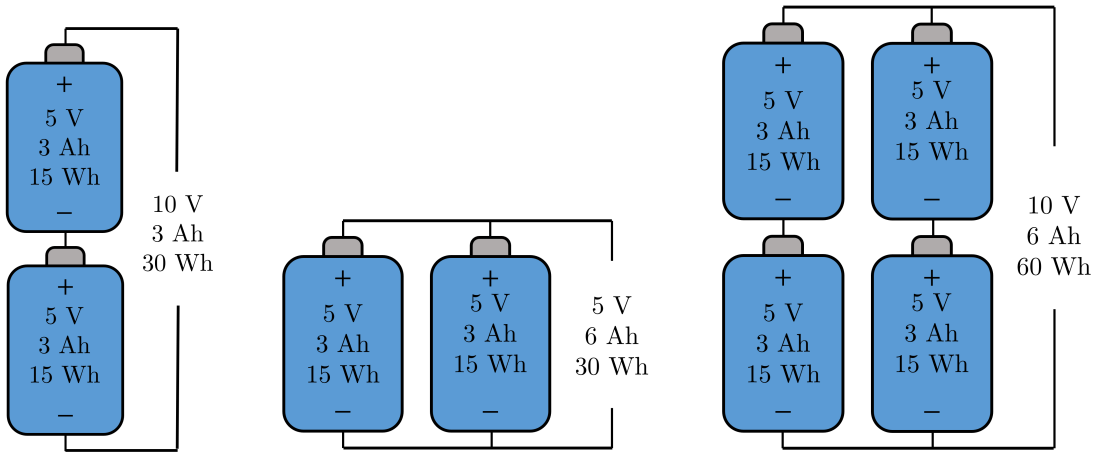

(a) Battery cells in series (1P2S).

(b) Battery cells in parallel (2P1S).

(c) Battery cells in parallel and series (2P2S).

Figure 2.6: Configuration of battery cells.

2.2 Thermal expansion

The thermal strain ε_T is calculated with

$$\varepsilon_T = \alpha(T)\,(T - T_0) - \alpha(T_0)\,(T_0 - T_{ref}) \tag{2.4}$$

where T is the current temperature, T_0 the initial temperature, T_{ref} the reference temperature for the thermal expansion coefficient and $\alpha(T)$ is the thermal expansion coefficient at temperature T. If $T_0 = T_{ref}$ Equation (2.4) can be simplified as

$$\varepsilon_T = \alpha \Delta T, \quad \Delta T = T - T_0 \tag{2.5}$$

2.3 Fluid expansion

Linear volume expansion of a fluid is calculated with

$$V(T) = V_0[1 + 3\alpha(T)(T - T_{ref}) - 3\alpha(T_0)(T_0 - T_{ref})] \tag{2.6}$$

where V_0 is the initial fluid volume, T_0 the initial temperature, T_{ref} the reference temperature for the thermal expansion coefficient and $\alpha(T)$ the secant coefficient of thermal expansion at temperature T. If α is temperature independent, Equation (2.6) can be simplified as

$$V(T) = V_0[1 + 3\alpha(T - T_0)] \tag{2.7}$$

2.4 Equivalent stiffness of springs in series

To estimate an equivalent material stiffness for different materials in series it is possible to use the theory of springs in series. According to this theory the equivalent spring stiffness K_{eq} is

$$\frac{1}{K_{eq}} = \sum_{i=1}^{n} \frac{1}{K_i} \tag{2.8}$$

for n linear springs in series. Figure 2.7 illustrates a system of n springs in series.

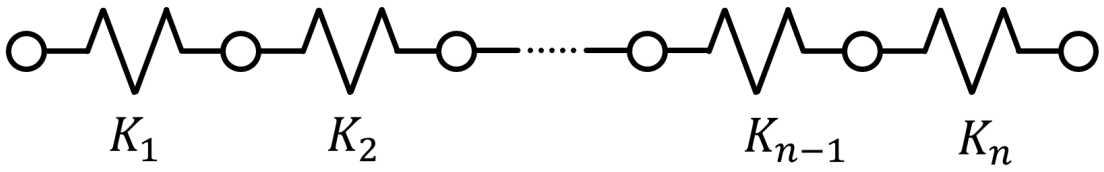

Figure 2.7: System of n springs in series.

3
Methods

3.1 M1: Swelling force

This section describes how a FE-model was set up to capture the swelling force of a battery cell, and how to fit the response to available physical test data.

3.1.1 Physical test data

The provided physical test data on swelling force was measured on the outside of the battery cell and is presented in Figure 3.1. The figure shows the normalised swelling force over number of cycles. The swelling force is normalised with the maximum measured force, obtained at 1500 cycles. The maximum swelling force is typically in the range $10 - 15$ kN [17]. We notice that about half of the total force arises within the first 150 cycles. Further we see that the force increases linearly over number of cycles after about 150 cycles.

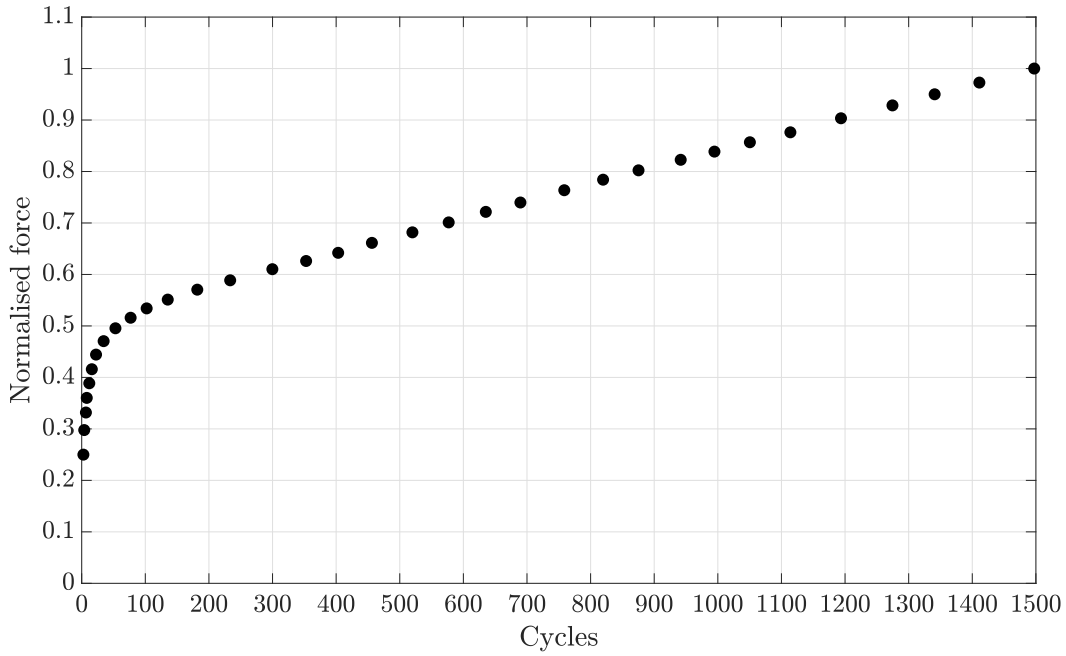

Figure 3.1: Physical test data on swelling force over number of cycles. The swelling force is normalised with the maximum measured force.

Figure 3.2 shows a schematic of how the test rig was set up when the physical test data on swelling force was measured. The battery cell was placed between two rigid plates as illustrated in the figure. The top plate was fixed while the bottom plate was allowed to slide vertically, i.e. in the y-direction. The force on the long sides of the cell, i.e. force in the y-direction, was measured with a force transducer located below the bottom plate.

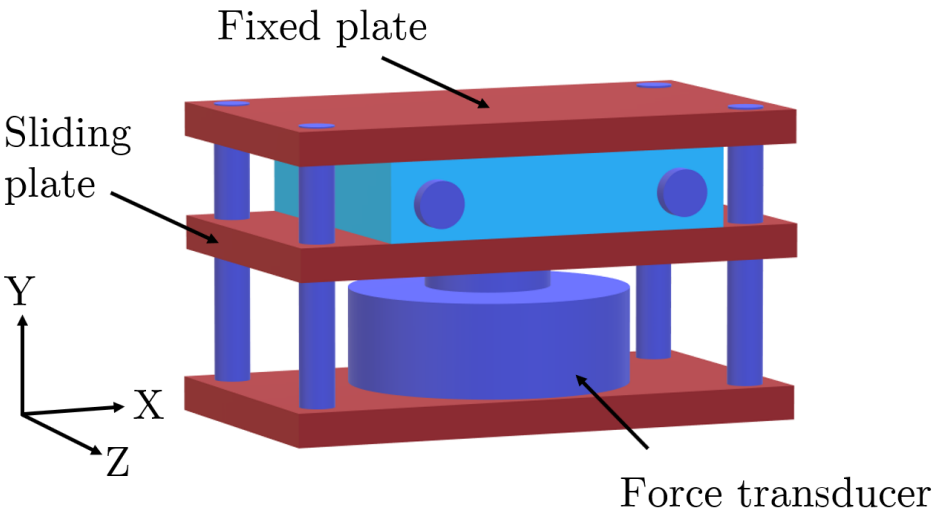

Figure 3.2: Schematic of the setup for the physical test measuring swelling force. Battery cell placed between two rigid plates with force transducer below.

3.1.2 FE-model setup

This section describes the different steps in the FE-model setup, e.g. how the mesh was set up and how the boundary conditions were defined. Figure 3.3 shows a 3D-schematic of the battery cell that was used in the FE analysis. The coordinate system shown in the figure was used throughout the project and is the one referred to when describing directions in the report.

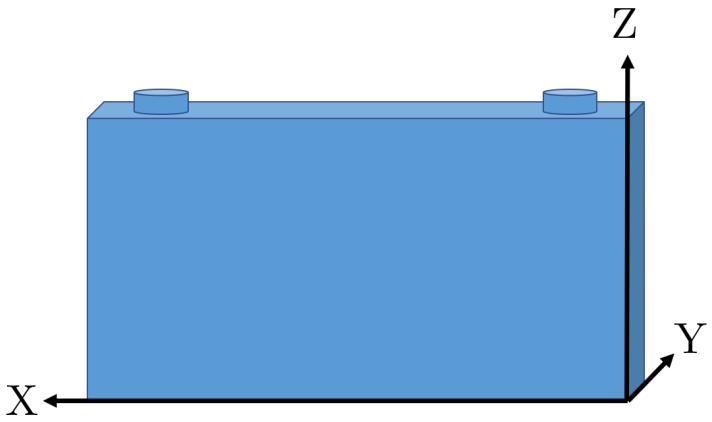

Figure 3.3: 3D-schematic of cell with coordinate system.

3.1.2.1 Number of cycles

The input to the FE-model was number of cycles. One cycle is defined as one complete charge and discharge cycle in this study. The studied span of cycles was limited to $0 - 1500$ cycles. Thermal expansion uses temperature as an input, hence an equivalent temperature was used to represent number of cycles in the FE-model. This means that an increase in cycles corresponds to a temperature increase. Here we set an equivalent temperature increase of 0.1°C per cycle. For example, an increase of 1000 cycles is equivalent to a 100°C temperature increase.

3.1.2.2 Geometry

The prismatic battery cell geometry used for the FE-model consisted of two jelly rolls, a casing and a top lid sealing the casing. Figure 3.4 shows schematics of cross-sections in two planes of the cell in Figure 3.3. The left figure illustrates the cross-section of the cell along the long side, i.e. in xz-plane. The right figure shows the cross-section along the width, i.e. in yz-plane. The dark grey area inside the casing illustrates the jelly rolls and the red areas on the top lid illustrates the positions of the terminals. These terminals, and parts linked to the terminals, were neglected in this study. Insulation parts such as insulation films, etc. were also neglected.

The relation between the width, height and length of the casing is highlighted in Figure 3.4. The width of the casing is defined as L. The height of the casing is double the width 2L, while the length is four times the width, 4L. The width of the battery cell is typically in the range $20 - 50$ mm [18]–[20] depending on the capacity of the cell. The casing bottom and wall thickness is denoted h, with the top lid being four times thicker than the walls, i.e. 4h.

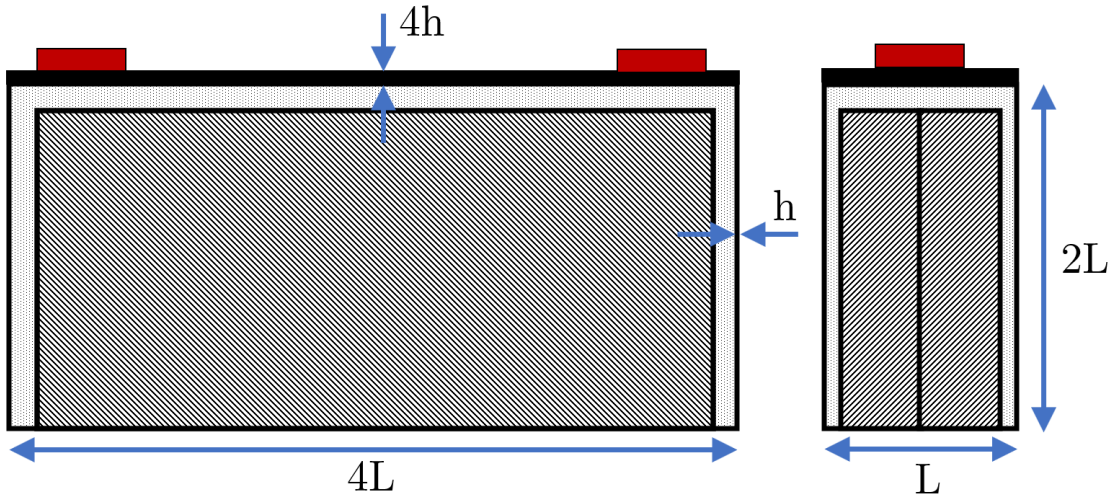

Figure 3.4: Schematic of battery cell cross-section. Left is cross-section in XZ-plane. Right shows cross-section in YZ-plane.

3.1.2.3 Mesh

The battery cell was meshed with a combination of solid and shell elements. The casing and lid were meshed using shell elements with 2 mm side length and their thickness corresponding to the real geometry, i.e. the lid is four times thicker than the casing. The jelly rolls were meshed with solid elements shaped as tetras and pyramids with 5 mm side length.

3.1.2.4 Materials

The casing was modelled with an aluminium material imported from a material database, which included plasticity and hardening data. The jelly rolls was modelled with Young's modulus E_{JR} and density from another FE-model of a battery cell. This material is about 1000 times softer than aluminium and was modelled as a linear elastic material, i.e. plasticity was not taken into consideration.

3.1.2.5 Thermal load

A temperature load was applied on the jelly rolls to obtain a thermal expansion. The initial temperature was set to 0°C, and it was then increased to 150°C. This temperature span was chosen since the physical test data for the swelling force is valid between $0 - 1500$ cycles. The magnitude of the temperature increments is dependent on the region of cycles. Looking at the physical test data in Figure 3.1, we see regions where the force increases non-linearly, and regions where it increases linearly with number of cycles. In the region where the force increase is non-linear, the temperature increments need to be smaller compared to regions where the force increase is linear. The temperature load was therefore divided into four steps.

Table 3.1 shows how the four steps were defined. The table shows the start temperature T_{start}, and the end temperature T_{end}, for each step. Each step is also divided into a number of temperature load increments, NoTLI. The last column in the table shows the magnitude of temperature load increments, TLI, and it is defined as

$$TLI = \frac{T_{\text{end}} - T_{\text{start}}}{NoTLI} \tag{3.1}$$

Table 3.1: The four steps of the thermal load used in the M1 method.

Step	$T_{\textbf{start}}$[°C]	$T_{\textbf{end}}$ [°C]	**NoTLI**	**TLI** [°C]
1	0	1	5	0.2
2	1	5	4	1
3	5	10	1	5
4	10	150	7	20

3.1.2.6 Boundary conditions

The boundary conditions in the FE-model were set to resemble the test rig setup shown in Figure 3.2. All nodes on the external surface of the long sides were coupled to a reference node located at the centre of the face as illustrated in Figure 3.5. This was performed on both sides of the casing. These reference nodes were fixed in all six degrees of freedom which fulfilled two purposes. The first was that the FE-model was constrained and the second purpose was that it made it possible to measure the reaction force on the long sides of the battery cell.

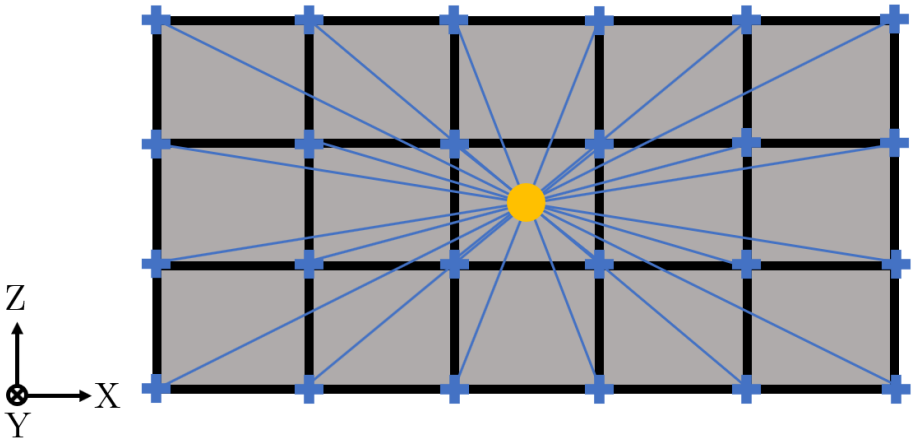

Figure 3.5: Illustration of how the nodes were coupled to a reference node on one long side of the battery cell.

3.1.2.7 Contact

A contact which ties the nodes on the contact surfaces was used to model the contact between the two jelly rolls. This contact definition will be referred to as *no-slip contact* in the report. The contact was defined on the inner surfaces of the jelly rolls to tie these two together. The jelly rolls were assumed to not slide against each other, leaving the friction out. This together with the fact that a *no-slip contact* is easier for the solver to handle was the reason that it was chosen here.

The jelly rolls expand due to the thermal load which implied a contact between the jelly rolls and the casing. This was modelled using a contact which allows slip and this contact definition will be referred to as *slip contact* in the report. An assumption of the magnitude of friction coefficient for the contact was made as $\mu = 0.3$. This assumption was based on the friction between two parts made from aluminium. In addition, an investigation of how the friction affects the response in terms of swelling force was performed. The small gap between the jelly rolls and the casing, seen in Figure 3.4, was closed by adjusting the contact. This was a way to obtain a response in reaction force right at the start of the simulation.

3.1.3 Parameter estimation

This section explains the different steps used to fit the swelling force curve provided to the project. The approach in this method was to use thermal expansion of the jelly rolls. The thermal expansion replicated the total swelling, including not only the thermal effects but also other swelling mechanisms e.g. gas build-up and SEI-layer growth. In other words, thermal expansion was used to replicate the total volume expansion.

The provided physical test data for the swelling force was measured only in y-direction as described in Section 3.1.1. Therefore, an orthotropic thermal expansion with $\alpha_x = \alpha_z = 0$ for the jelly rolls was assumed. This yields in an expansion only in y-direction where the swelling force is known from the physical test.

The first step in this method was to find the relation between the thermal strain on the jelly rolls, and the reaction force on the outside of the cell. This relation was then used to find which thermal strain, on the jelly rolls, that is needed to obtain a reaction force that replicates the measured swelling force in the physical test data. With known thermal strain at different number of cycles, the thermal expansion coefficient, α_y, was predicted at corresponding temperatures.

3.1.3.1 Strain-force relation

A reference model was set up to find the relation between the thermal strain on the jelly rolls and the reaction force on the outside of the case. This reference model used a constant thermal expansion coefficient and the temperature was increased with equally large increments.

Figure 3.6 shows the relation between the thermal strain on the jelly rolls and reaction force response on the outside of the casing from the FE-model. As shown in the figure the relation is linear and the strain can therefore be expressed as

$$\varepsilon_T = a \cdot F_{swell} + b \tag{3.2}$$

where F_{swell} is the swelling force, a is the slope of the curve and b is the thermal strain corresponding to zero force.

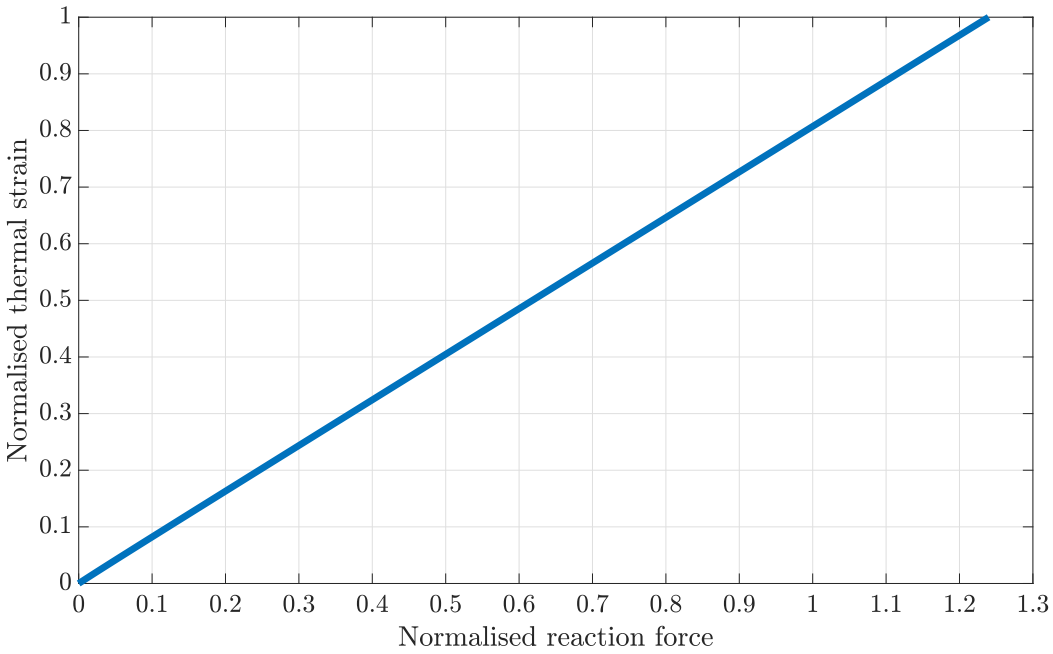

Figure 3.6: Normalised thermal strain vs. normalised reaction force. Thermal strain normalised with maximum strain and reaction force normalised with maximum measured swelling force from physical test data.

3.1.3.2 Thermal expansion coefficient prediction

The thermal expansion coefficient α_y for the jelly rolls was predicted with the relation

$$\alpha_y(T) = \frac{\varepsilon_T}{\Delta T} \tag{3.3}$$

where thermal strain ε_T was obtained from the strain-force relation in Equation (3.2). The temperature used to predict α_y was known from the physical test data shown in Section 3.1.1. The assumption that a 1°C temperature increase in the FE-model corresponds to an increase of ten cycles in the physical test data was used here to transform the number of cycles in the test data to an equivalent temperature used as input in Equation (3.3).

The thermal expansion coefficient for the jelly rolls depends on the applied temperature. The relation between α_y and the temperature, obtained from Equation (3.3), is shown in Figure 3.7, where α_y is normalised with the largest used value. This relation is only valid for the case when the physical test data shown in Section 3.1.1 is used.

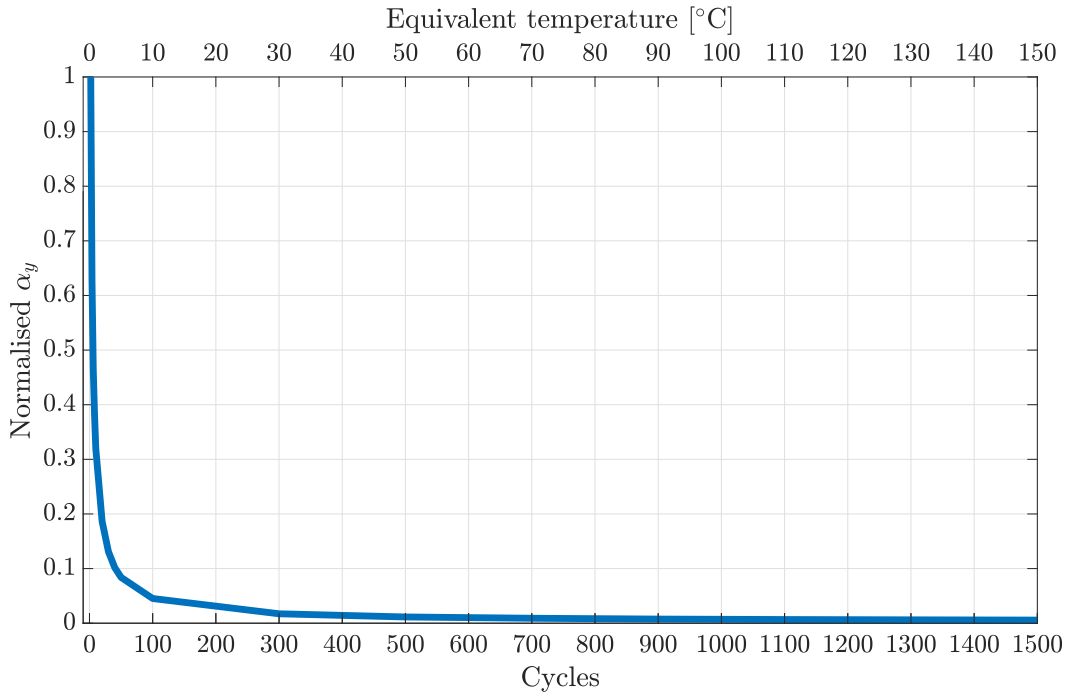

Figure 3.7: Normalised thermal expansion coefficient, α_y, as a function of the temperature applied on the jelly rolls.

3.2 M2: Gas pressure

This section describes how a FE-model was set up to predict gas pressure evolution in a battery cell, and how to fit the response to available physical test data.

3.2.1 Test data

The physical test data provided to this project consisted of gas pressure inside the battery cell over 15 years. The test data is obtained from testing battery cells with a usage profile that combines driving and parking, which means storage, charge and discharge are considered. Since the FE-model uses cycles as input an assumption of 250 cycles per year was made, i.e. 1500 cycles is equal to six years in Figure 3.8. This graph has the pressure normalised with the pressure in the cell at six years, which is typically in the range $0.1 - 0.2$ MPa [21]. The pressures of interest are the initial cell pressure P_1 and the pressure P_2 at 1500 cycles. Values for theses pressures are presented in Table 3.2.

Table 3.2: Normalised pressures of interest from physical test data. Pressures are normalised with the pressure at six years, i.e. 1500 cycles with an assumption of 250 cycles per year.

Pressure	**Value**
P_1	0.037
P_2	1

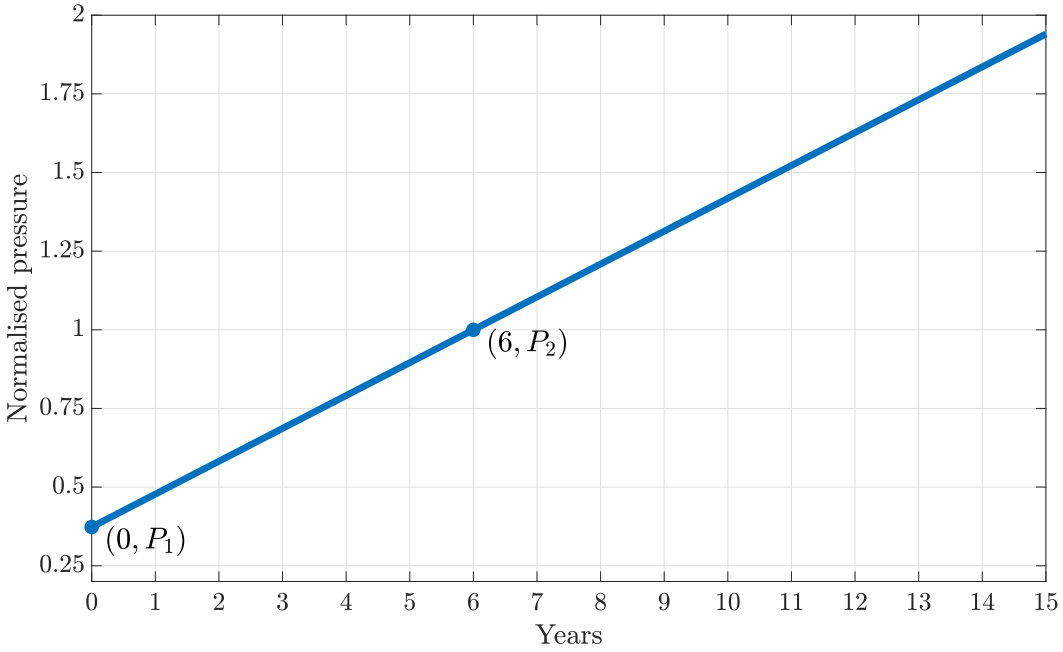

Figure 3.8: Experimental data of pressure build-up in a battery cell over 15 years. The pressure is normalised with the pressure at 1500 cycles, i.e. at six years with the assumption of 250 cycles per year.

The gas pressure inside the battery cell was measured from a setup with multiple cells stacked next to each other and the outer most cells clamped on the long sides, similar to the schematic in Figure 3.9. This setup was later considered when defining boundary conditions for the FE-model.

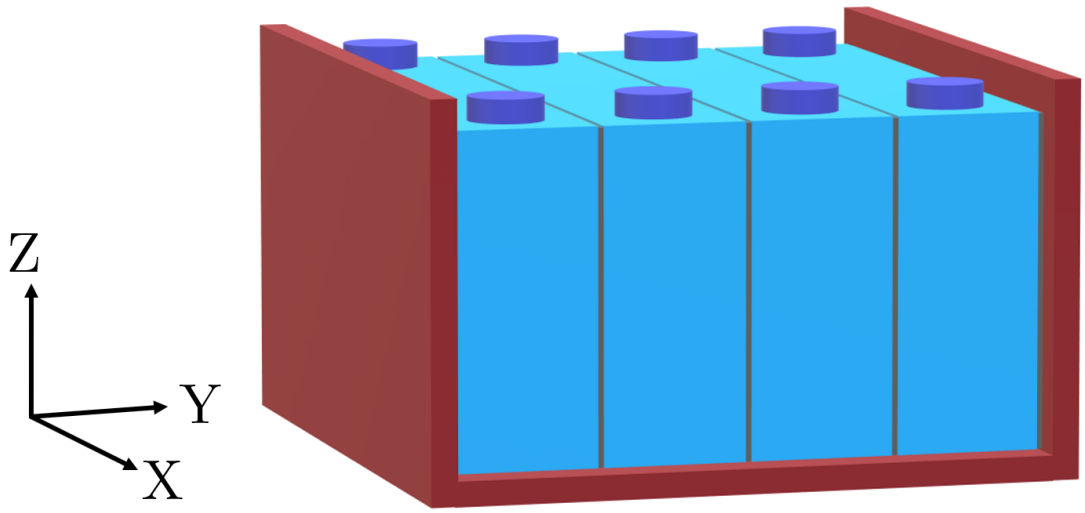

Figure 3.9: Schematic of cell configuration for gas pressure measurements.

3.2.2 FE-model setup

The M2 method used the same geometry, mesh and material parameters as the M1 method. This model did not have a thermal expansion of the jelly rolls, i.e. α_y was not used. An equivalent temperature that represented charge/discharge cycles was also the input for this FE-model. However, for this model a negative initial temperature T_0 was used to have the convenient relation with the conversion factor 10 between equivalent temperature change and increase in cycles.

3.2.2.1 Boundary conditions

Two types of swelling cases were tested with the gas pressure model to investigate the impact on the result from different boundary conditions: (i) constrained swelling; (ii) free swelling. The boundary conditions for the first case with constrained swelling resembled the test setup by having the long sides and bottom of the casing fixed as shown in Figure 3.10a. The boundary conditions for the second case was set up to represent free swelling of the battery cell. This was done by only having the lid fixed at the location of the battery terminals as shown in Figure 3.10b.

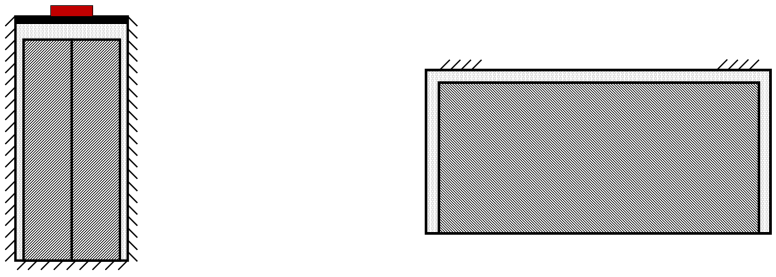

(a) Constrained swelling. **(b)** Free swelling

Figure 3.10: Different boundary conditions on a single cell for gas pressure simulations. (a) Boundary conditions representing the test setup with fixed sides and bottom of the casing. (b) Boundary conditions representing free swelling of the battery cell with the battery terminals fixed.

3.2.2.2 Gas modelling

In order to model gassing and to fit the gas pressure from the physical test data a cavity defined by a closed surface containing an incompressible fluid was modelled. The surface was defined by the casing and the outer surfaces of the jelly rolls. The fluid in the cavity is defined by its density, bulk modulus and thermal fluid expansion coefficient α. The bulk modulus and expansion coefficient can be defined as temperature dependent to capture non-linear behaviour. Gas generation over time was modelled as thermal volume expansion due to temperature increase of the fluid.

3.2.2.3 Thermal load steps

There was no initial gas pressure in the closed surface, which meant that two thermal load steps were necessary to define in the model. The first step started from the initial temperature T_0 and increasing to 0°C, and the second step started from 0°C increasing to 150°C. The first step makes sure that the pressure at 0°C is the same as the initial pressure P_1 from the physical test data, and the second step makes sure that the pressure in the cell reaches P_2.

3.2.3 Parameter estimation

To create a FE-model with similar gas pressure evolution as the physical test data the initial equivalent temperature T_0 and thermal expansion coefficient α were needed. The method to estimate these parameters through fluid volume, pressure and temperature is described below.

3.2.3.1 Volume-pressure relation

A reference model that captures the volume and pressure relation of the expanding fluid was set up. This model used boundary conditions from case (i) that reassembles the test setup, a sufficiently large constant α and the equivalent temperature range $0 - 150$°C, to reach pressures comparable with the physical test data.

The normalised pressure as function of equivalent temperature for the reference model is illustrated in Figure 3.11. In this figure the pressure is normalised with the pressure at 1500 cycles from the physical test data.

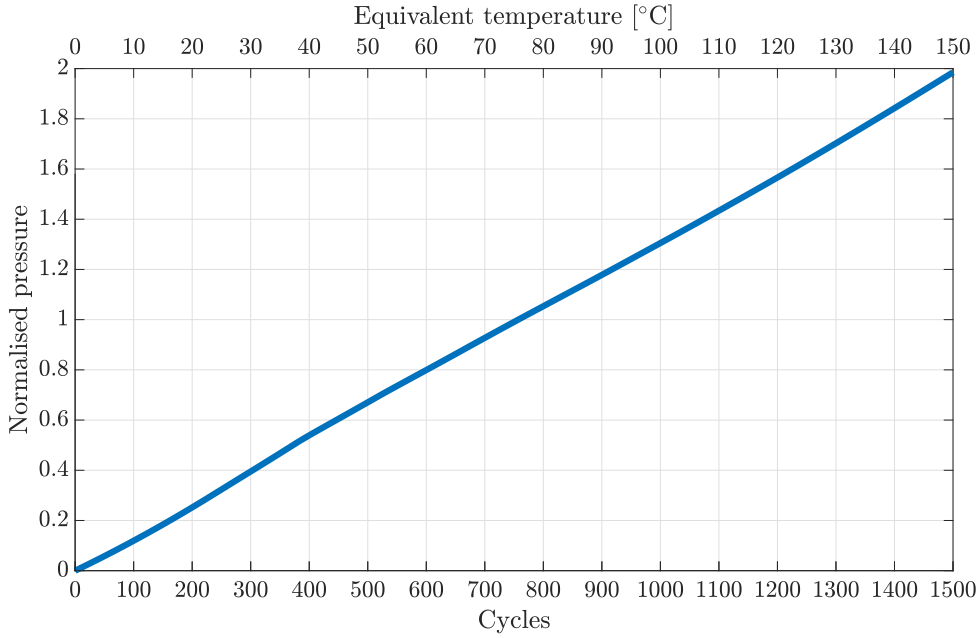

Figure 3.11: Normalised pressure and temperature relation from the reference model. The pressure is normalised with the pressure at 1500 cycles form the physical test data.

The normalised fluid volume as function of equivalent temperature is illustrated in Figure 3.12. The volume in this graph is normalised with the initial fluid volume.

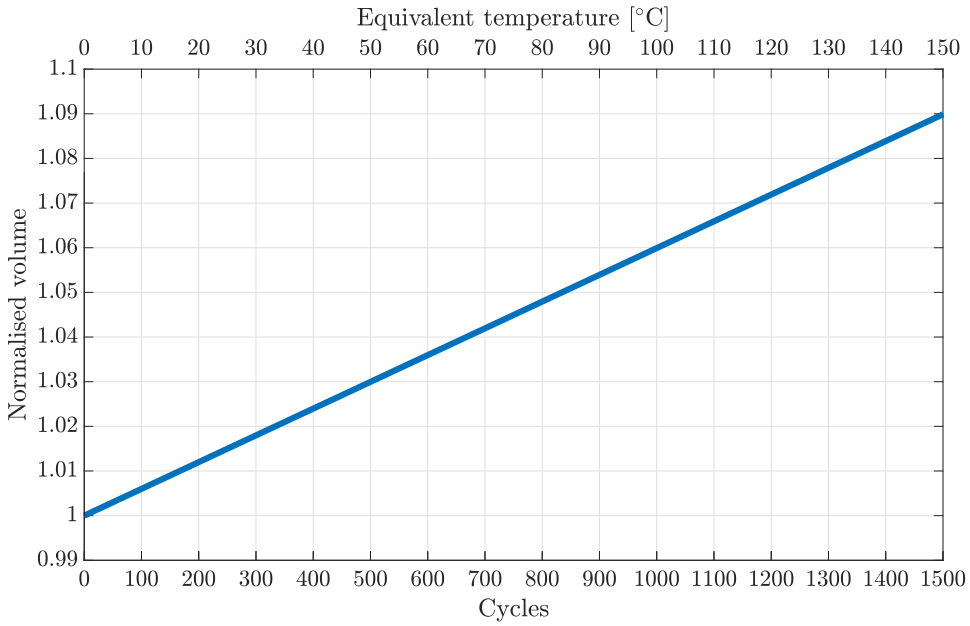

Figure 3.12: Normalised volume and temperature relation from the reference model. The volume is normalised with the initial fluid volume.

The volume vs. pressure was plotted in a graph to easily determine at what volume a certain pressure was obtained. The normalised fluid volume vs. pressure is shown in Figure 3.13.

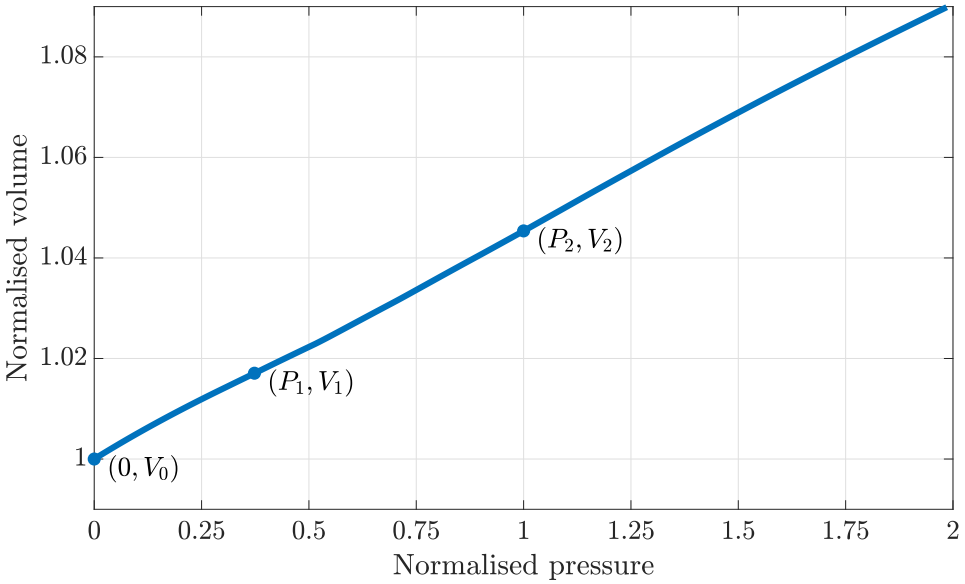

Figure 3.13: Normalised volume and normalised pressure relation. The volume is normalised with the initial fluid volume V_0 and the pressure is normalised with the pressure at 1500 cycles from the physical test data.

With the pressures of interest P_1 and P_2 described in Section 3.2.1 and the graph in Figure 3.13 it was possible to determine the volumes of interest, V_0, V_1 and V_2. The values are presented with a brief description of the volumes in Table 3.3.

Table 3.3: Normalised volumes of interest.

Volume	Value	Description
V_0	1	Initial fluid volume
V_1	1.017	Volume at pressure P_1
V_2	1.045	Volume at pressure P_2

3.2.3.2 Volume-temperature relation

Equation (2.7) in Section 2.3 describes the linear temperature and fluid volume relation. The linear relation makes it possible to create a curve using only two points. With the volumes V_0, V_1 and V_2, and the temperatures T_1 and T_2 known, the slope of the linear curve ranging from point (T_1, V_1) to (T_2, V_2) can be calculated. Further, the equivalent initial temperature $T_0 = -90.44$°C was determined using the slope and the volume V_0 in a linear equation. This is illustrated in Figure 3.14. The reason for using a negative T_0 is to have a convenient conversion factor between equivalent temperature change and cycle increase for all the models in this project.

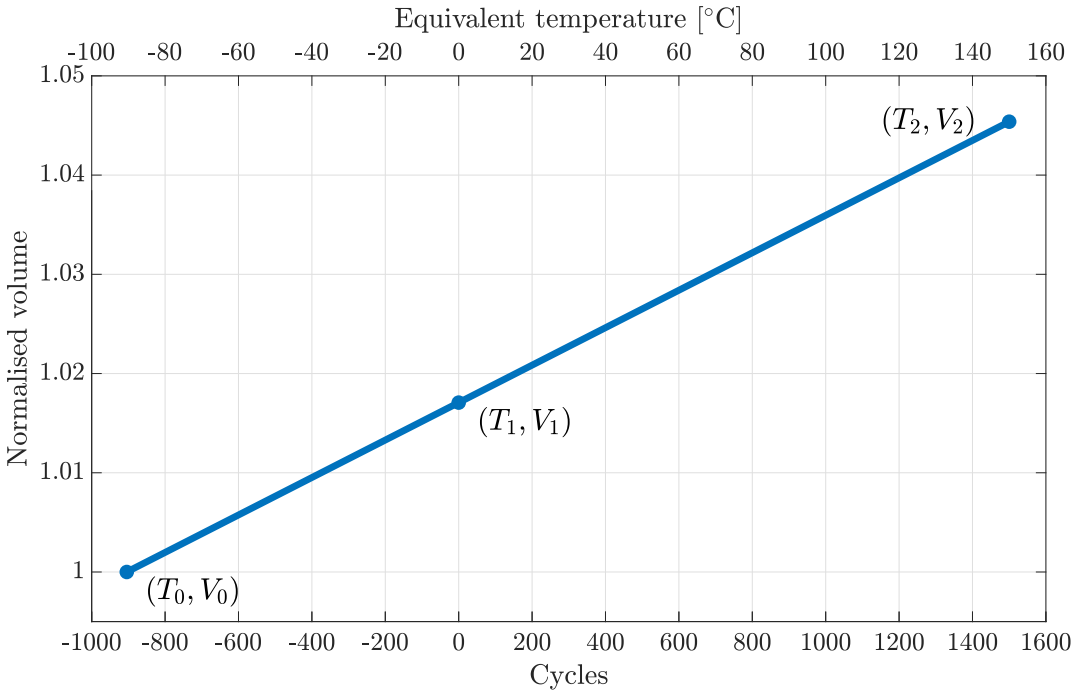

Figure 3.14: Normalised volume and temperature relation used to determine initial temperature T_0.

Since the pressure increases linearly a constant α was assumed. Equation (2.7) was rearranged to solve for α as

$$\alpha = \frac{V/V_0 - 1}{3\Delta T} \tag{3.4}$$

and could then be used in the FE-model.

3.3 M3: Simplified geometry

The simplification of the M1 model consisted of a changed geometry. A solid block with only one material in the same outer dimensions as the original cell was used, instead of the casing and jelly rolls. The mesh also differs from M1, the element side length is 5 mm and the volume was meshed with rectangular prism elements.

A large portion of the setup was similar to the M1 concept. However, the simplified model did not require contacts which reduced the computational time. The thermal load and boundary conditions were set up in the same way as in the M1 model. The thermal expansion coefficient α_y from M1 was also used in M3.

3.3.1 Material

The material used for the solid block was determined using the theory of springs in series, i.e. aluminium and jelly roll material was combined to an equivalent material. The aluminium had a very small impact on this equivalent material stiffness due to it being significantly stiffer than the jelly roll material. The equivalent material stiffness differed by less than 1% from the jelly roll material. Thus, the softer material governs the equivalent stiffness of springs in series.

3.3.2 Parameter estimation

Using the jelly roll material from the M1 model for the simplified geometry resulted in a larger reaction force compared to the M1 method, see Figure 3.15.

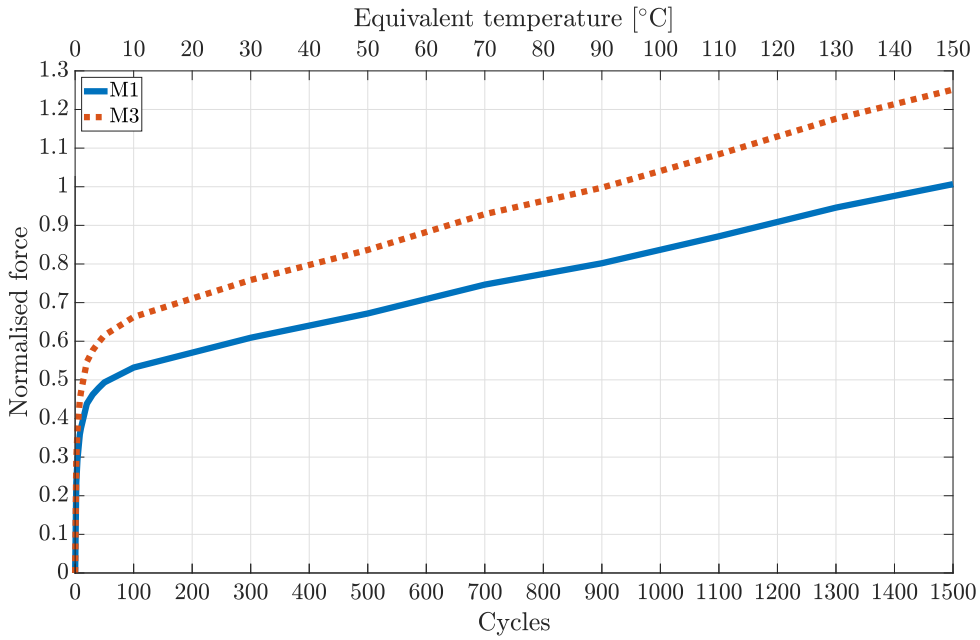

Figure 3.15: Force comparison of M1 and M3 methods using the same material parameters.

To adjust this the Young's modulus or α_y was scaled with the scale factor S_f. This scale factor was determined by the area relation

$$S_f = \frac{A_{contact}}{A_{face}} \tag{3.5}$$

where $A_{contact}$ is the contact area of the jelly roll and A_{face} is the face area of the solid block.

The reason why the scale factor is based on the areas is the difference in deformation of the side face for the two geometries. During thermal expansion the solid block has a uniform displacement over the entire side face. On the other hand, the casing in the M1 method has a non-uniform deformation when the jelly rolls are thermally expanded, due to the edges of the casing stiffening up the structure. The largest displacements would be obtained near and on the contact area of the jelly roll, and the displacements would decrease when moving towards the edges of the casing. The displacements are related to the reaction force at their particular nodes, thus the solid block will have a larger total sum of reaction forces compared to the M1 cell. Hence, the reaction forces from the M3 cell must be reduced to fit the test data. It is possible to use the same scale factor for both α_y and Young's modulus due to the material model, thermal strain equation etc. being linear. With a non-linear material model, e.g. considering plasticity, it might not be possible to use the same scale factor for both α_y and Young's modulus.

3.4 M4: Battery module

This section describes the method for modelling a complete module in a battery pack. A detailed module containing multiple cells and foam pads was set up. Figure 3.16 illustrates a schematic of the battery module including these components. The detailed module model was simplified by neglecting the terminals and the busbars shown in the figure.

The module geometry was extracted from a battery pack model where it was already meshed. The battery cell geometry in this model differed slightly from the geometry in M1 method. Therefore, a new strain-force relation also had to be investigated to reduce the impact from these differences. Finally, the method on how this module was simplified using a solid block will also be described.

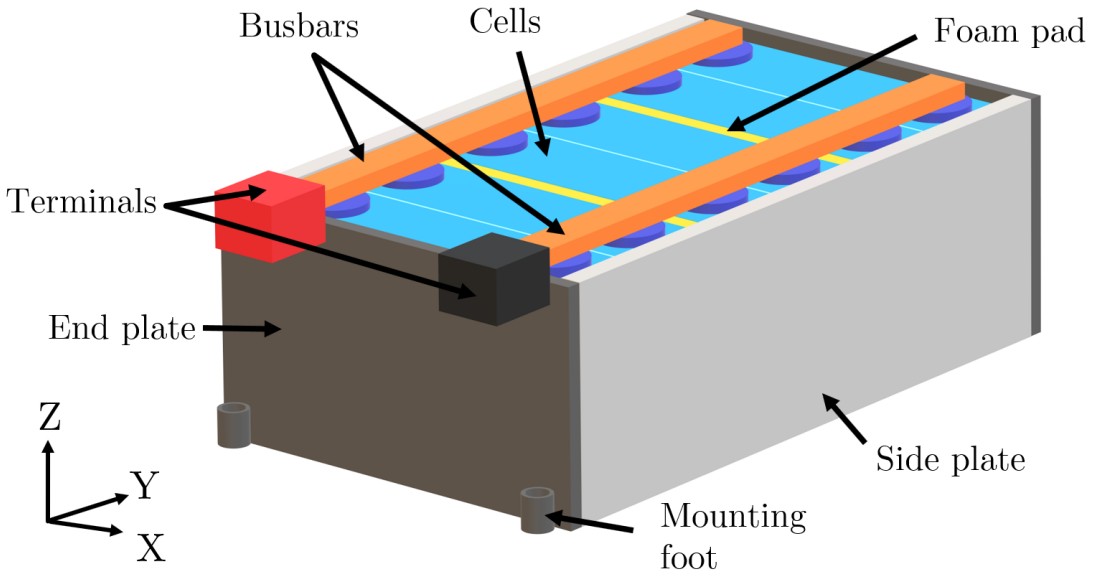

Figure 3.16: Schematic of the detailed battery module used in battery packs.

3.4.1 Test data

The available data on the module was displacement of the end plates due to cell swelling. An increase of the initial module length was measured from another FE-model. Due to confidentiality these results cannot be presented. The input for this model was swelling forces on the cells in the y-direction. These are not the same swelling forces as presented for the M1 method in Figure 3.1. The normalised swelling forces on the cells used as input for the module model are presented in Figure 3.17. The forces were measured in a similar test rig as shown in Figure 3.2. The forces in the graph are normalised with the maximum swelling force from Section 3.1.1 to make them comparable with all other forces presented in this report.

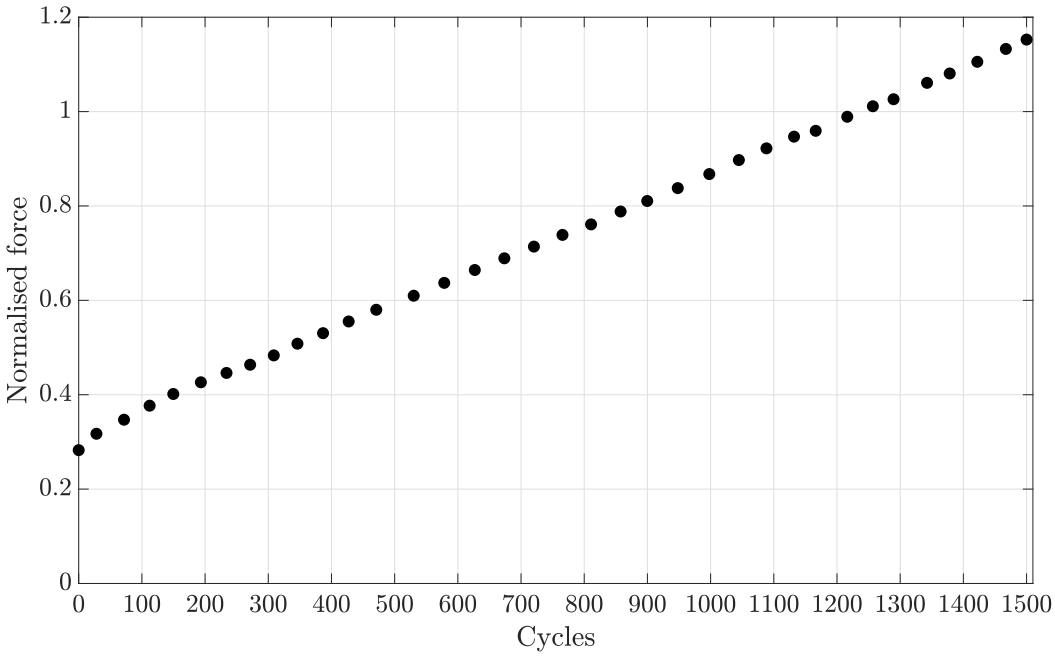

Figure 3.17: Normalised swelling forces on cell used in physical test of complete module. Swelling forces are normalised with the maximum measured force from Section 3.1.1.

3.4.2 FE-model setup of detailed module

The FE-model of a detailed battery module was set up with an already meshed geometry. The input to the model was number of cycles. Similar to the other models created in this project, the increase in cycles was represented by an equivalent temperature increase that was used with thermal expansion to model the cell swelling.

3.4.2.1 Mesh

The geometry was meshed using a mix of shell elements, solid elements and a type of elements used for gaskets. Cell casing, end plates and side plates used shell elements, the mounting feet and jelly rolls used solid elements. Foam pads were meshed with an element type used for gaskets, this type of elements consider the non-linear behaviour of the foam material.

3.4.2.2 Materials

The battery cell casings, side plates and end plates are all made of aluminium. The casings and side plates were defined with a stronger aluminium material than the end plates. The jelly rolls used the same material definition as in M1. Young's modulus of the jelly rolls was also scaled up with factors 10 and 100, due to the module length increase being very small when using $E = E_{JR}$ for the jelly rolls.

3.4.2.3 Foam pads

The foam pads are very soft compared to the parts next to them in the module. Modelling the foam pads with solid continuum elements is difficult with this large difference in stiffness. There is a major risk of obtaining negative volumes of the foam pads when a pressure from the swelling is applied. The foam pads were therefore modelled in a similar way to gaskets, using an element type which does not use a regular material model but instead requires a closure-pressure relation. Figure 3.18 shows the closure-pressure behaviour used for the foam pads in the detailed module model. The closure-pressure relation was provided from a physical test and it describes how much the thickness will close when a certain pressure is applied.

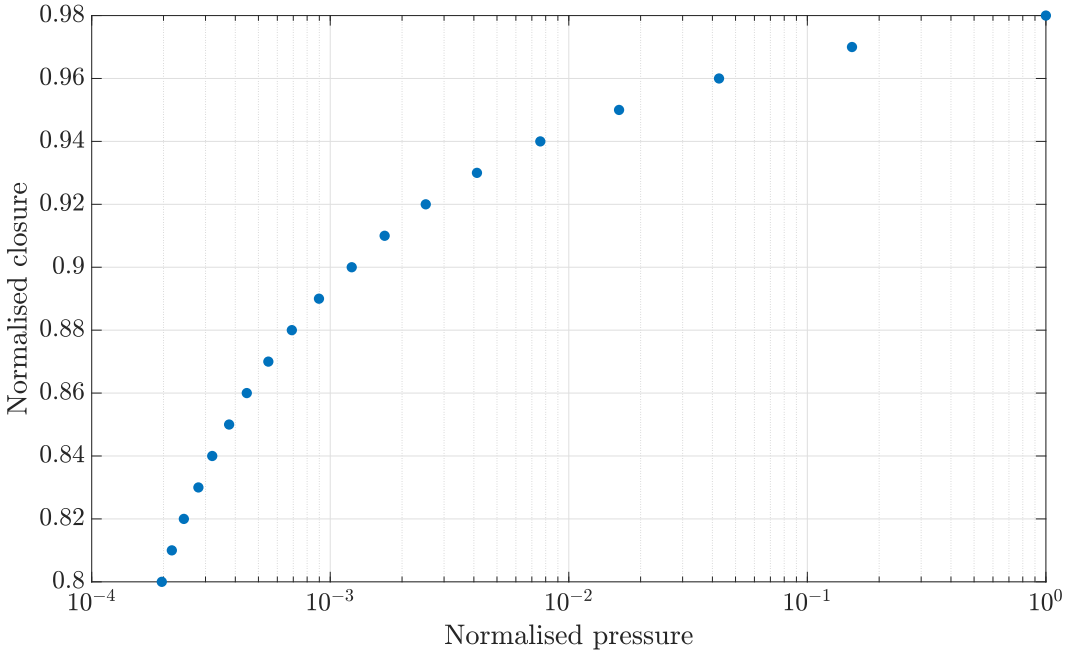

Figure 3.18: Closure-pressure relation for the foam pads in the FE-model. Closure normalised with initial thickness of foam pads. Pressure normalised with maximum pressure applied in test.

3.4.2.4 Boundary conditions

The nodes inside the bolt holes located in the mounting feet were fixed in all translations and rotations to resemble the module being mounted in the battery pack. The bottom of the cells were constrained in z-direction and all three rotations, i.e. they were free to move in x- and y-direction.

3.4.2.5 Contacts

The contact between cells, foam pads and end plates in the detailed module was modelled using multiple *no-slip contacts*, one for each contact. The short sides of the cells were connected to the side plates with *no-slip contact* as well. The contact was defined on the entire short side to model glue pads that holds the cell in the module, and prevent penetration between the side plates and cells.

3.4.2.6 Load

The load on the module originates from cell swelling. The swelling of the cells was modelled with thermal expansion of the jelly rolls similar to the M1 method. The steps in the M1 method were used to find the proper $\alpha_y(T)$ for the jelly roll material to replicate the swelling behaviour presented in Figure 3.17. A new strain-force relation was created to take the differences in the battery cell geometry into consideration. All cells were assumed to swell with the same swelling behaviour, i.e. all jelly rolls used the same material properties.

The physical test data of swelling force over number of cycles for the cells used in the module differed from the data used in M1. The swelling force curve for this case shows a linear behaviour which means that the resolution for $\alpha_y(T)$ can be reduced compared to M1. Hence, the number of steps was reduced to two steps and these are stated in Table 3.4.

Table 3.4: The two steps of the thermal load used on the cells in the module.

Step	T_{start}[°C]	T_{end} [°C]	NoTLI	TLI [°C]
1	0	10	10	1
2	10	150	14	10

3.4.3 Simplified module

The detailed module was simplified by replacing the battery cells and the foam pads with a solid block. This solid block is referred to as cell block in the report and Figure 3.19 shows the module with the cell block. The cell block has an equivalent bulk material that corresponds to the materials in the cells and foam pads. The methods on how the material parameters for this bulk material was approximated is presented in this section, together with the model setup.

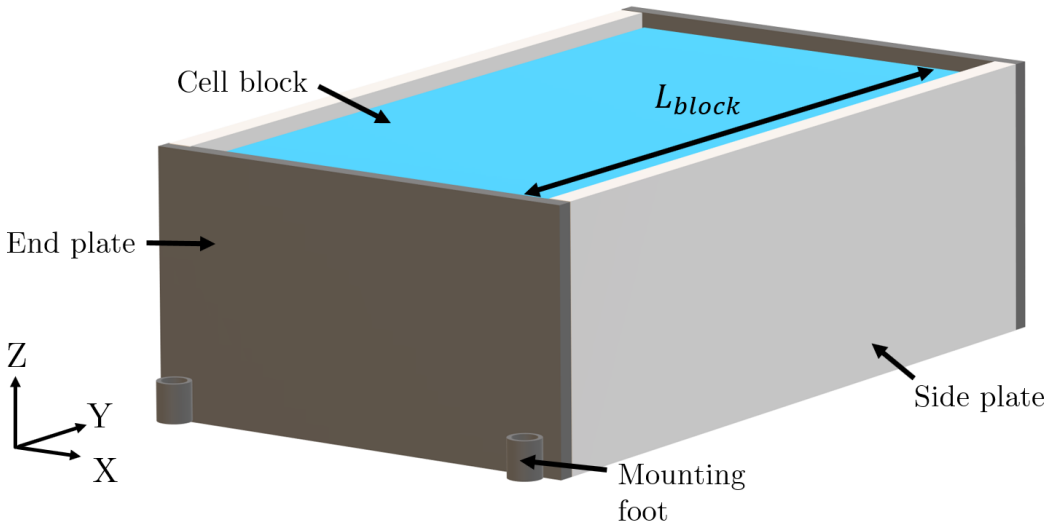

Figure 3.19: Schematic of the simplified battery module.

The boundary conditions and thermal load was set up the same way for both the detailed and simplified module. This was performed to make the detailed and simplified models comparable. Both models used the same $\alpha_y(T)$.

3.4.3.1 Contacts

The cell block had *no-slip contacts* defined between the side plates and the long side faces of the block to prevent penetration. There were also *no-slip contacts* defined between the end plates and the cell block.

3.4.3.2 Material approximation

A bulk material stiffness for the cell block was approximated using three different methods: (i) the theory of springs in series; (ii) assuming the cell block consisted of only jelly roll material; (iii) cell block and battery cell length ratio.

Case (i) combined the stiffness of aluminium, the jelly roll and the foam material into an equivalent stiffness with the theory of springs in series. Since the foam material varies with the degree of compression it was assumed that it had the constant stiffness of a fully compressed foam pad, which is about 50% of the jelly roll stiffness.

Case (ii) assumed that the solid block consisted of only the jelly roll material, since the jelly rolls are the only parts that thermally expands in the model.

Case (iii) used the scale factor

$$S_f = \frac{2 \cdot L}{L_{block}} \tag{3.6}$$

to scale down the stiffness of the cell block, where L is the battery cell width and L_{block} is the initial length of the block in the y-direction. This scale factor was used on: (iii-a) the equivalent stiffness from case (i); (iii-b) on the jelly roll stiffness.

The reasoning for this scale factor is that the major contribution to the displacements of the end plates comes from the outer most cells. The idea is that swelling of the inner cells mostly cancel each other out, due to the cell casings being adhered to the side plates with *no-slip contacts*.

4

Results

4.1 M1: Swelling force

The reaction force on the large faces of the battery cell obtained in the FE-model is plotted in Figure 4.1 together with the physical test data on swelling force. The forces in the figure are normalised with the maximum obtained swelling force from the physical test.

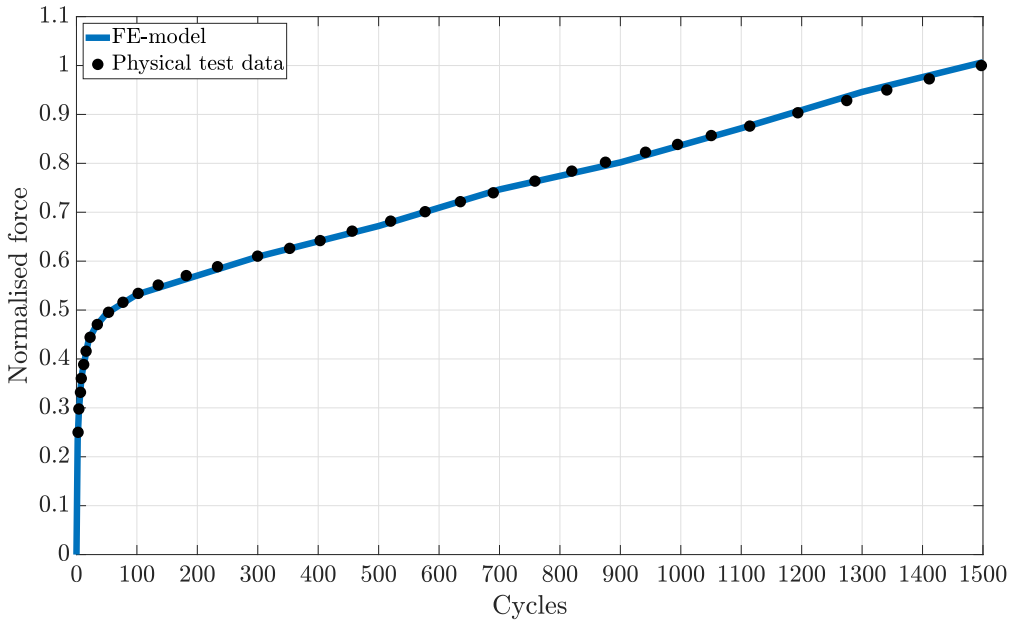

Figure 4.1: Reaction force from FE-model fitted to the swelling force from the physical test data. The forces are normalised with the maximum swelling force obtained at 1500 cycles.

Different friction coefficients for the contact between the jelly rolls and the casing were tested. Figure 4.2 shows the fitted FE-model using three different friction coefficients. The curve corresponding to $\mu = 0.3$ is the same curve as in Figure 4.1. The figure shows that a very low, close to zero, friction coefficient yields a noticeable change in the reaction force. However, increasing the friction coefficient does not affect the reaction force in this case.

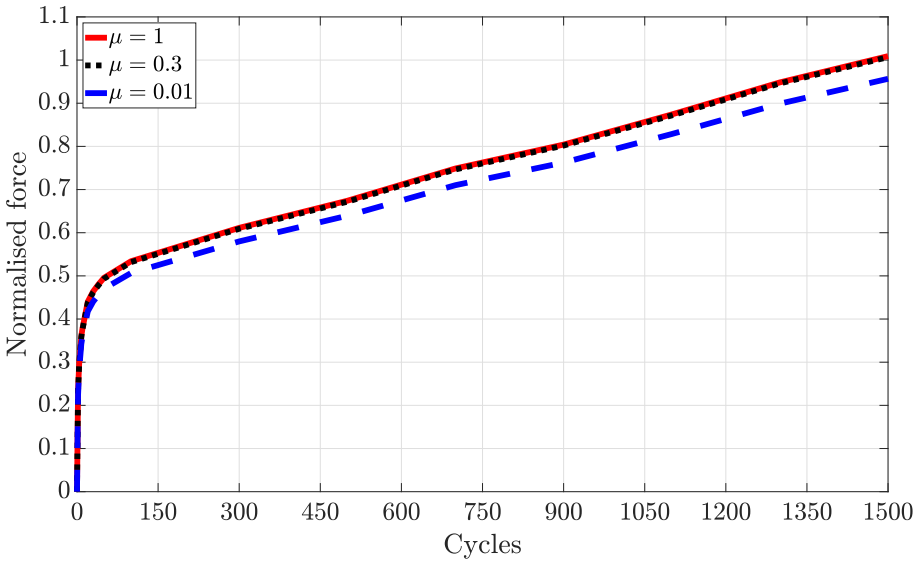

Figure 4.2: Fitted FE-model with different friction coefficients for the contact between the jelly rolls and the casing. Force normalised with the maximum force from the physical test data.

4.2 M2: Gas pressure

Figure 4.3 shows a comparison of the physical test data and the model prediction using the FE-model. From the figure it can be seen that the FE-model captures the gas pressure increase. In this figure the pressure is normalised with the pressure at 1500 cycles from the physical test data. The part of the orange curve that ranges from about -900 to 0 cycles corresponds to the first step of the FE-model.

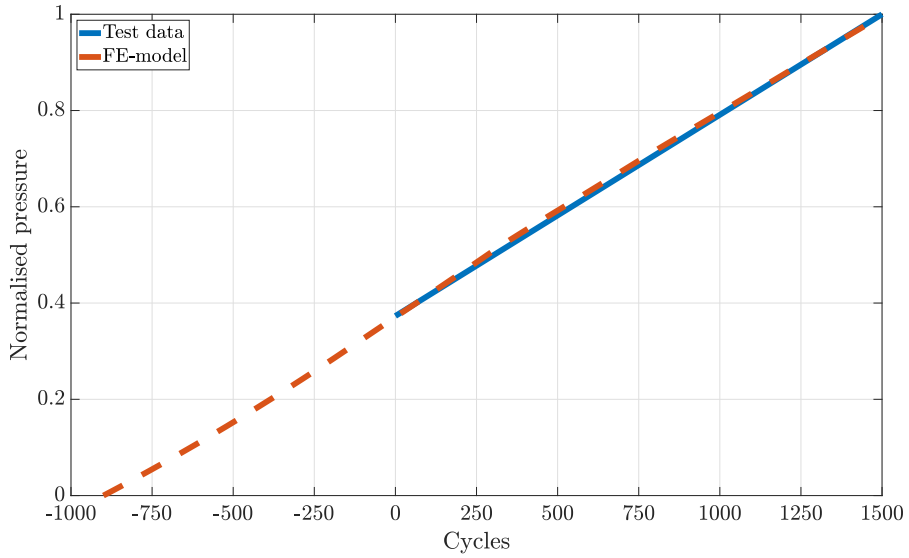

Figure 4.3: FE-model results compared with physical test data. The pressure is normalised with the pressure at 1500 cycles from the physical test data.

Figure 4.4a shows a comparison of the gas pressures in the battery cells with boundary conditions representing constrained and free swelling. This figure shows a pressure that appears to be constant zero for the boundary conditions representing free swelling. Further, Figure 4.4b shows only the curve with the normalised gas pressure for the boundary condition representing free swelling, to clarify that the pressure also increases for this case.

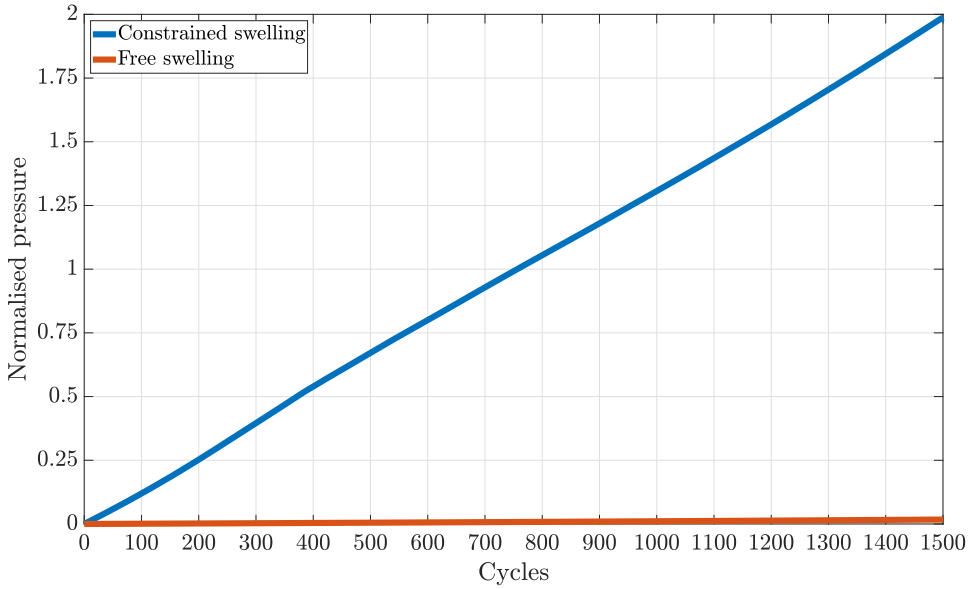

(a) Constrained and free swelling.

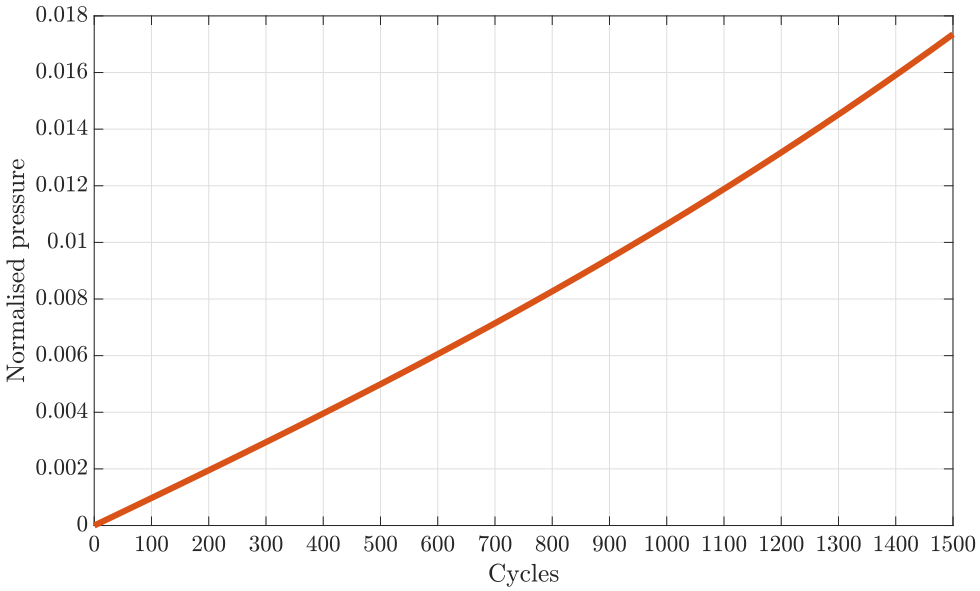

(b) Free swelling.

Figure 4.4: Comparison of different boundary condition effects on gas pressure. (a) Comparison of gas pressure evolution with constrained and free swelling of the battery cell. (b) Gas pressure evolution in the free swelling battery cell. The pressures are normalised with the pressure at 1500 cycles from the physical test data.

4.3 M3: Simplified geometry

Figure 4.5 shows a comparison of the normalised swelling forces between the M1 and M3 concept. From this graph it is also possible to compare the effects from scaling the Young's modulus and α_y with the scale factor S_f.

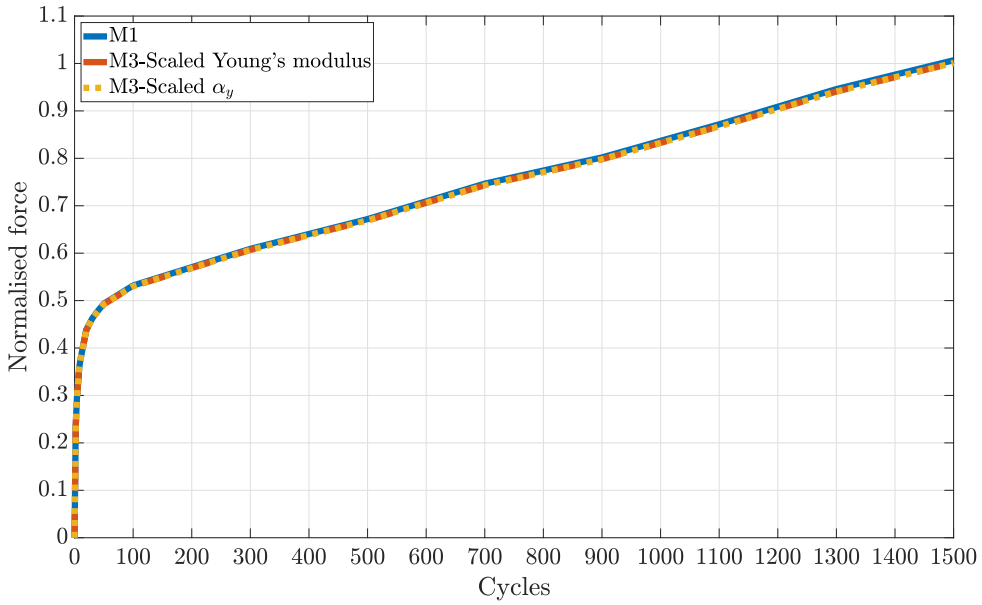

Figure 4.5: Comparison of normalised swelling forces between the full and simplified geometry. The forces are normalised with the maximum swelling force obtained at 1500 cycles.

4.4 M4: Battery module

Table 4.1 shows the result for the detailed module model. The first column displays the jelly roll stiffness in the model. The second column displays the module length increase as a percentage of the maximum module length increase from the test data.

Table 4.1: Length increase of detailed module model for different jelly roll stiffness.

Stiffness	Percentage of test data
E_{JR}	20%
$10 \cdot E_{JR}$	29%
$100 \cdot E_{JR}$	32%

With the Young's modulus for the jelly rolls increased by a factor 100, plastic strains up to roughly 13% could also be observed in the side plates near the foam pads. Figure 4.6 shows a schematic of the deformed shape, where the red oval highlights the region where plastic strains were observed.

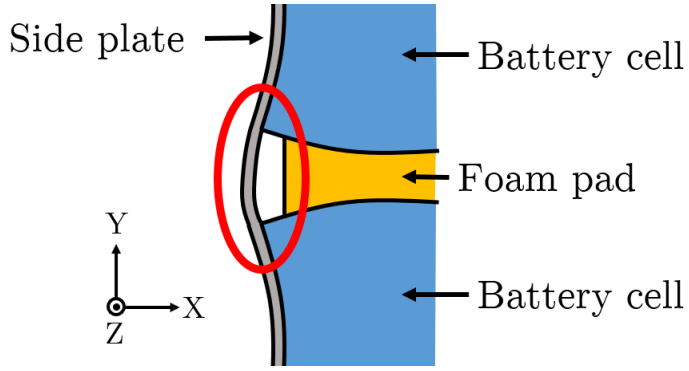

Figure 4.6: Schematic of deformed side plate and battery cells. The region where plastic strains were observed is highlighted in the red oval.

Table 4.2 shows the result for the simplified module. The first column displays the approach that was used to determine the bulk material stiffness. The second column displays the module length increase as a percentage of the module length increase from the detailed module model using the non-scaled Young's modulus, i.e. $E = E_{JR}$. The simplified module did not exhibit any plastic strains in the side plates.

Table 4.2: Length increase of simplified module model for different bulk material stiffness.

Bulk material stiffness	**Percentage of detailed module length increase**
Springs in series	203%
Jelly roll stiffness	326%
Scaled springs in series	52%
Scaled jelly roll stiffness	131%

5
Conclusions and discussion

5.1 M1: Swelling force

Using method M1 shows that the reaction force from the FE-model coincides well with the physical test data. The method is able to capture the swelling force behaviour both in the linear and the non-linear region.

The reference model showed a linear relation between the thermal strain on the jelly rolls and the reaction force. The reference model used a constant α_y which results in a linear expansion of the jelly rolls. The battery cell was also fixed on the large faces of the casing meaning that the geometry of the battery cell do not contribute to a non-linear relation. Due to lack of data a linear elastic material was assumed for the jelly rolls which also contributed to the linear relation observed. It should be considered that the stiffness of the jelly rolls will vary when swelling occur in the cell and that in reality the large faces will not be completely fixed. The conclusion here is that this linear relation is a special case due to the assumptions that have been made. However, even if the relation is non-linear it can be used to estimate the thermal expansion coefficient.

The physical test data for the swelling force provided to the project was limited to swelling force on the large faces of the battery cell, i.e. in y-direction. It was therefore decided to only have expansion of the jelly rolls in y-direction. One option would be to use the same expansion in both x- and y-direction for the jelly rolls with the argument that there are as many layers of electrodes on the short sides of the jelly rolls as there are on the long sides. However, it cannot be verified that this is the case without any data connected to the short sides of the cells. It was therefore decided to assume expansion only in the y-direction.

The presented M1 method can be used to fit data in both directions for the same cell. However, it will result in a more complex problem to solve since the reaction force on one side will be coupled to the other. During this study, displacements at the short sides of the casing have been noticed without any expansion in this direction. Due to Poisson's effects, defined by the Poisson's ratio of the material, a deformation in the y-direction causes a resultant deformation in the x-direction. An additional expansion in the x-direction will therefore be affected of the expansion in the y-direction. Thus, applying expansion in both directions will yield in a coupled problem where the two swelling forces need to be fitted at the same time.

The model of the battery cell in the M1 method contained contacts. The contact between the jelly rolls and the case walls allowed slip. A friction coefficient for this contact was therefore required but since it was unknown it had to be assumed. The assumption of $\mu = 0.3$ was based on data for friction between two aluminium parts. An additional study on how the friction coefficient for the contact affected the results was performed. The conclusion from this study is that a lower friction coefficient than the assumed will influence the result and therefore a proper friction coefficient for this contact needs to be considered in future studies.

5.2 M2: Gas pressure

When looking at the curve in Figure 4.3 we find that the FE-model predicts the gas pressure from the physical test data well. There are some small non-linear deviations in the gas pressure of the FE-model that may be explained by non-linear behaviour in the geometry, e.g. curved deformations due to corners of the casing. The method gives a good approximation when modelling gas pressure evolution. It was easy to fit the model to the available test data, considering the linear pressure increase. Although, there should not be any problem fitting the model to a non-linear pressure evolution using the M2 method.

It is also possible to include swelling of the jelly rolls, since the volume change of these have an impact on the fluid volume and therefore impacts the gas pressure. Thus, making it possible to combine the swelling effects from gas pressure build-up and other sources of swelling, e.g. intercalation or thermal effects.

Looking at how the gas pressure differed between constrained and free swelling, it is obvious that the boundary conditions have a large impact on the result. If the gas pressure evolution is of interest, the boundary conditions must be properly defined to make the results relevant.

5.3 M3: Simplified geometry

With a simplified geometry it is possible to reduce the needed computational resources, due to fewer contacts and meshed parts, and still get a similar response in reaction force. However, the simplified geometry has drawbacks. If the boundary conditions were different to the fixed sides, the deformations would differ when comparing the M1 and M3 cell, as described in Section 3.3. The geometrical simplification by using a solid block may not be suitable if the deformed shape is important to the application. If there would be swelling deformations in more than one direction the different geometries might also have an effect on the results. Due to the limited amount of test data, expansion in multiple directions was not investigated. Frictional effects, like shearing between the casing and jelly roll in the M1 method is also difficult to consider with a solid block. The effects on the results by changing the geometry to a solid block needs to be investigated further to be sure it is a suitable replacement in FE-models.

The method of using springs in series theory to determine an equivalent material response for the simplified geometry worked well in combination with the scale factor. Although, the aluminium being significantly stiffer than the jelly roll material caused it to have a negligible effect on the equivalent stiffness. Therefore, uncertainties emerged on how well the method would work for other material combinations. Due to the lack of data on the jelly roll material it was assumed to be linear elastic with a constant stiffness, although it is known that the stiffness changes over the life span. There are also e.g. unknown plasticity and potentially viscoelastic effects for the jelly rolls that need to be considered. If these parameters were known it is necessary to consider them when creating an equivalent material for the solid block, and in that case the springs in series theory might be unsuitable.

5.4 M4: Battery module

The detailed module utilised the M1 method to estimate α_y used to replicate the cell swelling. The reaction force on the cell coincided well with the physical test data provided for this case. This verifies that the M1 method is a good approach to model swelling forces on the battery cell.

The detailed module did not predict the test data well. The module length increase was roughly 20% of the test data for the case when using $E = E_{JR}$. Even with an increase of Young's modulus on the jelly rolls by a factor 100 the resulting module length increase was only 32% of the test data, which is far from a desired result. An acceptable difference between the models could be a $\pm 10\%$ difference in length increase. Therefore, the model must be set up in a different way to be more accurate.

With the jelly roll stiffness increase, plastic strains were observed on the side plates where the foam pads are located. These strains can be explained by the *no-slip contacts*. In reality the glue will have an adhesive effect up to a certain failure point, and then allow slip between the different parts. The glue would fail before the aluminium shows signs of plastic strains. With glue pads allowing slip, a larger module length increase is also expected to occur since the battery cells would be allowed to move in the y-direction. The detailed module was simplified by removing the busbars and terminals, it is expected that they would change the structural stiffness if they were included. This is something to study further since anything that changes the structure is of interest.

The simplified module did not reproduce the results from the detailed module well. When comparing results from the detailed and simplified module it was found that the length increase varies largely. The simplified module differed from roughly half the length increase up to three times as large as the detailed module, depending on the method used to approximate the bulk material. The method that came closest had a 30% larger length increase of the module compared to the detailed model. The difference in response between the models is significant and cannot be neglected. Thus, the method to determine a bulk material needs further investigation.

Since strain is related to the initial dimensions it is not surprising that the long solid block caused a larger length increase of the module. This length must somehow be considered when setting up the FE-model, as this model showed it was possible to change the displacements by scaling the Young's modulus. By using a different α_y it is also possible to affect the displacement, something that was not tested in this project.

Following the previous reasoning, a *no-slip contact* is not an accurate representation of reality when slip is expected in the contact. An expansion of the block in the y-direction will then cause a length increase of the side plates, contributing to the total length increase of the module. Therefore the contact between the solid block and side plates must be further investigated.

Generally, the contact definition for both module models is uncertain. The reason for using *no-slip contacts* was the FE-solvers ability to obtain convergence more easily with this contact definition. Contacts that were allowed to slip was tested but the FE-solver was not able to solve them properly, and the simulations terminated early. Due to the module being the last thing modelled in this project lack of time meant further work on the model was not performed. The model that was developed in this project also had different boundary conditions compared to the model where the module length increase was measured. The mounting feet in that module model were connected to bases with pre-tensioned bolts with contacts between the feet and bases allowing slip. This type of boundary condition was not set up due to lack of time, but is recommended in further studies.

5.5 Future work

This section presents suggestions and ideas for future work with FE-modelling of battery cell swelling. Additionally, suggestions on valuable experimental data for future studies are presented.

For future work with capturing the swelling in a FE-model it would be convenient to have all the physical test data, that are to be fitted, measured on the same battery cell. The cycling curve of the cell in the tests should also be the same. This would make the results more comparable in the analysis step. It would also be convenient if the same cells then are used when physical tests are to be done in a complete module.

The model set up in the M1 method contained a fixed boundary condition on the long sides. When continuing the work with this model it needs to be investigated how this boundary condition can be changed. An investigation of how the model can be set up to allow some displacements and still obtain the reaction force is recommended, i.e. without allowing it to expand freely.

Another suggestion for future work is to combine the two methods, M1 and M2. Using the thermal expansion of the jelly rolls from M1 and the fluid expansion from M2. A combined model would be useful when one is interested in separating the different swelling sources. The internal gas pressure would be represented by the fluid expansion and the remaining sources would the be represented by the thermal expansion of the jelly rolls. This would be useful when studying swelling of one single cell rather than a complete module or battery pack. In this case the complete swelling of the battery cell is of interest, and how that affects the surrounding parts in the module, e.g. the module structure.

Parameters for the fluid in the M2 method were assumed to be similar to incompressible air. For future modelling of gas pressure evolution, it is of interest to investigate how other fluid parameters than α affect the results. It would also be of interest to compare deformations on battery cells due to gas pressure build-up, which requires test data on these deformations.

It was possible to fit the swelling forces using a simplified battery cell geometry in the M3 method. Since the deformations were not evaluated with this model it is difficult to say if the geometry change is valid for any other case or boundary conditions. This is something that needs to be determined before simplifications can be used in a larger scale.

The detailed module model largely underestimated the length increase, even when increasing the Young's modulus of the jelly rolls. Further work with this type of problem would be to model the contacts in a more accurate way. With the contacts more accurately defined a study on which jelly roll stiffness resulting in the same length increase should be performed. If the material parameters are fixed, e.g. when the model is used in a crash simulation with particular material parameters, it is possible to alter the swelling behaviour by changing α_y. This was not tested in this project but is of interest in future work.

The simplified module overestimated length increase compared to the detailed module. The methods tested to approximate the bulk material resulted in large deviations of the module length increase. Further studies should be done to find a way to define this bulk material. Similar to the detailed module, the contacts need a more realistic definition. It is also of interest to investigate if there are any structured methods to modify α_y to have similar results from both module models.

5.5.1 Experimental data for future work

This project had limited amount of physical test data and during the project it became clear what types of data that could be useful in order to perform a more detailed study in the future. This section will therefore present suggestions on useful experimental data for future work with FE-modelling of battery cell swelling.

It was discussed earlier in the report that expansion of the jelly rolls in more than one direction would replicate reality better. This would require test data for the swelling force on all sides of the battery cell. These measurements need to be performed at the same time to intercept the coupled behaviour as discussed. An additional data on displacements of the cell would be preferable. Knowing the relation between the displacement and the swelling force would be very useful for future work with replicating the swelling in FE-models.

The M1 method was developed to replicate the swelling force on the long sides of the battery cell. This swelling force occurred due to many factors as discussed earlier. The M2 method, replicated the gas pressure inside the battery cell. This gas pressure was one of the factors included in the swelling force for M1. A suggestion would be to perform a physical test where the swelling force and the gas pressure are measured at the same time. This data would be useful if further studies to set up a FE-model which combines the two methods.

There have been uncertainties in this project regarding the friction coefficient between the jelly rolls and the casing. A physical test measuring the correct friction coefficient between these two components would be valuable data when further investigation is performed. Further it is known that the stiffness properties of the jelly rolls vary over time when the battery cell is cycled. This will have an impact on the swelling force and therefore it needs to be measured and captured in the model.

Bibliography

[1] I. Tsiropoulos, D. Tarvydas, and N. Lebedeva, "Li-ion batteries for mobility and stationary storage applications - scenarios for costs and market growth," EUR 29440 EN, Luxembourg, Publications Office of the European Union, 2018. DOI: http://dx.doi.org/10.2760/87175.

[2] W. Chen, J. Liang, Z. Yang, and G. Li, "A review of lithium-ion battery for electric vehicle applications and beyond," *Energy Procedia*, vol. 158, pp. 4363–4368, 2019, Innovative Solutions for Energy Transitions. DOI: 10.1016/j.egypro.2019.01.783.

[3] A. Bhatt, M. Forsyth, R. Withers, and G. Wang. (2016). "How a battery works," [Online]. Available: https://www.science.org.au/curious/technology-future/batteries (visited on Mar. 11, 2021).

[4] H. Berg, *Batteries for Electric Vehicles: Materials and Electrochemistry*. Cambridge University Press, 2015. DOI: 10.1017/CBO9781316090978.

[5] B. Wu, Y. Yang, D. Liu, C. Niu, M. Gross, L. Seymour, H. Lee, P. Le, T. Vo, Z. Deng, E. Dufek, M. Whittingham, W. Liu, and J. Xiao, "Good practices for rechargeable lithium metal batteries," *Journal of The Electrochemical Society*, vol. 166, A4141–A4149, Dec. 2019. DOI: 10.1149/2.0691916jes.

[6] T. Woehrle, "Lithium-ion cell," in *Lithium-Ion Batteries: Basics and Applications*, R. Korthauer, Ed. Berlin, Heidelberg: Springer Berlin Heidelberg, 2018, pp. 101–111. DOI: 10.1007/978-3-662-53071-9_9.

[7] *Bu-301a: Types of battery cells*. [Online]. Available: https://batteryuniversity.com/learn/article/types_of_battery_cells (visited on Mar. 18, 2021).

[8] N. Sato, "Thermal behavior analysis of lithium-ion batteries for electric and hybrid vehicles," *Journal of Power Sources*, vol. 99, no. 1, pp. 70–77, 2001. DOI: 10.1016/S0378-7753(01)00478-5.

[9] M. A. Gialampouki, J. Hashemi, and A. A. Peterson, "The electrochemical mechanisms of solid–electrolyte interphase formation in lithium-based batteries," *The Journal of Physical Chemistry C*, vol. 123, no. 33, pp. 20 084–20 092, 2019. DOI: 10.1021/acs.jpcc.9b03886.

[10] N. E. Galushkin, N. N. Yazvinskaya, and D. N. Galushkin, "Mechanism of gases generation during lithium-ion batteries cycling,"
Journal of The Electrochemical Society, vol. 166, no. 6, A897–A908, 2019.
DOI: 10.1149/2.0041906jes.

[11] S. S. Zhang, "Insight into the gassing problem of li-ion battery,"
Frontiers in Energy Research, vol. 2, p. 59, 2014.
DOI: 10.3389/fenrg.2014.00059.

[12] M. Rashid and A. Gupta, "Mathematical model for combined effect of SEI formation and gas evolution in li-ion batteries,"
ECS Electrochemistry Letters, vol. 3, no. 10, A95–A98, 2014.
DOI: 10.1149/2.0041410eel.

[13] B. Rowden and N. Garcia-Araez, "A review of gas evolution in lithium ion batteries," *Energy Reports*, vol. 6, pp. 10–18, 2020.
DOI: 10.1016/j.egyr.2020.02.022.

[14] *What is lithium plating?* [Online]. Available:
https://www.upsbatterycenter.com/blog/lithium-plating/ (visited on Mar. 17, 2021).

[15] S. A. Roberts, H. Mendoza, V. E. Brunini, B. L. Trembacki, D. R. Noble, and A. M. Grillet, "Insights into lithium-ion battery degradation and safety mechanisms from mesoscale simulations using experimentally reconstructed mesostructures," *Journal of Electrochemical Energy Conversion and Storage*, vol. 13, no. 3, 2016. DOI: 10.1115/1.4034410.

[16] T. L. Kulova, "Effect of temperature on reversible and irreversible processes during lithium intercalation in graphite,"
Russian Journal of Electrochemistry, vol. 40, no. 10, pp. 1052–1059, 2004.
DOI: 10.1023/B:RUEL.0000046490.73990.c3.

[17] Y. Li, C. Wei, Y. Sheng, F. Jiao, and K. Wu, "Swelling force in lithium-ion power batteries," *Industrial & Engineering Chemistry Research*, vol. 59, no. 27, pp. 12 313–12 318, 2020. DOI: 10.1021/acs.iecr.0c01035.

[18] *LiFePO4/Li-Ion Battery Cells: 3.7V 50Ah NCM Prismatic Li-ion Battery Cell for EV*, OSN Power Energy Limited. [Online]. Available:
https://www.osnpower.com/3-7v-50ah-ncm-prismatic-li-ion-battery-cell-for-ev_p39.html (visited on May 17, 2021).

[19] A. S. Mussa, "Durability aspects of fast charging, mechanical constraint, and inhomogeneity in lithium-ion batteries,"
Doctoral thesis, KTH The Royal Institute of Technology, 2018.

[20] H.-K. Kim, J. H. Choi, and K.-J. Lee, "A numerical study of the effects of cell formats on the cycle life of lithium ion batteries,"
Journal of The Electrochemical Society, vol. 166, no. 10, A1769–A1778, 2019.
DOI: 10.1149/2.0261910jes.

[21] J. Schmitt, B. Kraft, J. P. Schmidt, B. Meir, K. Elian, D. Ensling, G. Keser, and A. Jossen, "Measurement of gas pressure inside large-format prismatic lithium-ion cells during operation and cycle aging,"
Journal of Power Sources, vol. 478, p. 228 661, 2020.
DOI: 10.1016/j.jpowsour.2020.228661.

DEPARTMENT OF INDUSTRIAL AND MATERIALS SCIENCE
CHALMERS UNIVERSITY OF TECHNOLOGY
Gothenburg, Sweden
www.chalmers.se

CHALMERS
UNIVERSITY OF TECHNOLOGY